

# **Performance of Transuranic-Loaded Fully Ceramic Micro- Encapsulated Fuel in LWRs Final Report, Including Void Reactivity Evaluation**

R. Sonat Sen  
Michael A. Pope  
Brian Boer  
Abderrafi M. Ougouag  
Gilles Youinou

September 2011

The INL is a U.S. Department of Energy National Laboratory  
operated by Battelle Energy Alliance



# **Performance of Transuranic-Loaded Fully Ceramic Micro-Encapsulated Fuel in LWRs Final Report, Including Void Reactivity Evaluation**

**R. Sonat Sen  
Michael A. Pope  
Brian Boer  
Abderrafi M. Ougouag  
Gilles Youinou**

**September 2011**

**Idaho National Laboratory  
Fuel Cycle Research & Development  
Idaho Falls, Idaho 83415**

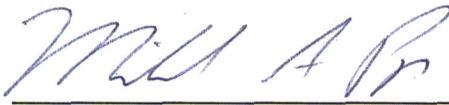
**<http://www.inl.gov>**

**Prepared for the  
U.S. Department of Energy  
Office of Nuclear Energy  
Under DOE Idaho Operations Office  
Contract DE-AC07-05ID14517**

#### **DISCLAIMER**

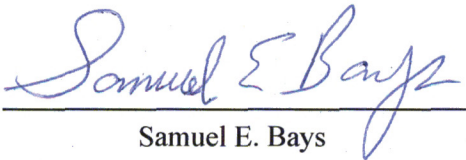
This information was prepared as an account of work sponsored by an agency of the U.S. Government. Neither the U.S. Government nor any agency thereof, nor any of their employees, makes any warranty, expressed or implied, or assumes any legal liability or responsibility for the accuracy, completeness, or usefulness, of any information, apparatus, product, or process disclosed, or represents that its use would not infringe privately owned rights. References herein to any specific commercial product, process, or service by trade name, trade mark, manufacturer, or otherwise, does not necessarily constitute or imply its endorsement, recommendation, or favoring by the U.S. Government or any agency thereof. The views and opinions of authors expressed herein do not necessarily state or reflect those of the U.S. Government or any agency thereof.

**Co-Authors:**

 9/19/2011

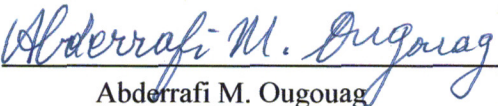
Michael A. Pope for R. Sonat Sen,      Date  
Brian Boer, Abderrafi M. Ougouag,  
and Gilles Youinou

**Reviewed by:**

 9/19/11

Samuel E. Bays      Date

**Concurred by:**

 09/19/2011

Co-Author and Work Package Manager

Abderrafi M. Ougouag      Date

Page Intentionally Left Blank

## **ACKNOWLEDGEMENTS**

The authors would like to gratefully acknowledge Vincent Descotes, Alain Hébert, and Guy Marleau of École Polytechnique de Montréal for their assistance in using the DRAGON-4 code throughout the Deep Burn project.



## SUMMARY

The current focus of the Deep Burn Project is on once-through burning of transuranics (TRU) in light-water reactors (LWRs). The fuel form is called Fully-Ceramic Micro-encapsulated (FCM) fuel, a concept that borrows the tri-isotropic (TRISO) fuel particle design from high-temperature reactor technology. In the Deep Burn LWR (DB-LWR) concept, these fuel particles are pressed into compacts using SiC matrix material and loaded into fuel pins for use in conventional LWRs. The TRU loading comes from the spent fuel of a conventional LWR after 5 years of cooling.

Unit cell and assembly calculations have been performed using the DRAGON-4 code to assess the physics attributes of TRU-only FCM fuel pins in an LWR lattice. Depletion calculations assuming an infinite lattice condition were performed with calculations of various reactivity coefficients performed at each step. Unit cells and assemblies containing typical  $\text{UO}_2$  and mixed oxide (MOX) fuel were analyzed in the same way to provide a baseline against which to compare the TRU-only FCM fuel. Then, assembly calculations were performed evaluating the performance of heterogeneous arrangements of TRU-only FCM fuel pins along with  $\text{UO}_2$  pins.

The main objective of this report is to give results of the following activities:

- Evaluate reactivity-limited burnup of TRU-only FCM fuel cells in a Pressurized Water Reactor (PWR)
- Calculate key reactivity coefficients, including total coolant void coefficient, of the TRU-only FCM fuel at various levels of depletion and evaluate the effects of varying the kernel size and packing fraction (PF) on these coefficients
- Compare these results to reference  $\text{UO}_2$  and MOX unit cells
- Perform similar calculations on heterogeneous FCM/ $\text{UO}_2$  assembly configurations, again evaluating reactivity-limited burnup and reactivity coefficients.

In addition to the above mentioned goals, a companion report [B. Boer, et. al., FCR&D-2011-000338 or INL/EXT-11-23313 reports on use of the PASTA code to evaluate the integrity of FCM fuel for normal operation states at various levels of depletion and in a simulated LOCA transient.

It was shown that due to the limited space available for heavy metal loading within the FCM fuel, the reactivity-limited burnup (in days) at typical LWR power densities may be short compared to ordinary LWR cycle lengths if only the FCM fuel is used. Thus, even before evaluating the reactivity feedback performance of the fuel, it was recognized that the idea of using heterogeneous assemblies containing pins of TRU-only FCM alongside pins with low-enriched uranium (LEU) deserved consideration.

The reactivity parameters calculated versus depletion were the Moderator Temperature Coefficient (MTC), the void coefficient (assuming 10% void), the Doppler coefficient, the soluble boron worth, and the reactivity effect of complete voiding of the coolant. This was done for single unit cells of TRU-only FCM fuel followed by heterogeneous assemblies containing arrangements of both.

### *Unit Cell Calculations*

Several different combinations of TRISO particle packing fractions (PF) and kernel diameters were evaluated for the FCM fuel. It was found that the total heavy metal (HM) loading of the FCM fuel is the primary driver for reactivity-limited burnup and for reactivity coefficients, not how it is distributed in various kernel sizes and PF values. The MTC of the TRU-only FCM fuel was negative at beginning of life, but *less so* than the MTC of  $\text{UO}_2$  and MOX reference cases. With burnup, the MTC becomes less negative, and in the cases with very small fuel loading, eventually turns positive. The evaluated case with the smallest amount of fuel (500  $\mu\text{m}$  diameter kernel, PF=20%, 0.21  $\text{g}/\text{cm}^3$  TRU) exhibits a positive MTC when burnup reaches about 200 GWd/tonne. This is because so little heavy metal remains that the system



becomes over-moderated. However, HM loadings this small are also undesirable from the standpoint of TRU destruction rates. In other cases, with higher HM loading, the MTC becomes positive at higher burnup levels. The likelihood of reaching such high levels of burnup is low.

The calculations of the void coefficient assuming 10% void show similar results relative to the  $\text{UO}_2$  and MOX reference cases. The value of this parameter for the TRU-only FCM fuel was negative at beginning of life, but less so than in the  $\text{UO}_2$  and MOX reference cases. With burnup, it becomes less negative, and in the cases with very small fuel loading, turns positive at higher burnups. The evaluated case assuming the smallest amount of fuel (500  $\mu\text{m}$  diameter kernel,  $\text{PF}=20\%$ ,  $0.21 \text{ g/cm}^3$  TRU) gives a positive value at a burnup level around 400 GWd/tonne. Again, higher loadings than this are more desirable for TRU destruction reasons and a positive 10% void coefficient could be easily avoided.

The Doppler coefficient of the fresh TRU-only FCM fuel is between  $-0.6$  and  $-1.2 \text{ pcm}/^\circ\text{C}$ . With burnup, the magnitude of this coefficient for all FCM cases decreases until a value of 0 is reached at higher burnup levels. The burnup at which this occurs, as for the cases of the MTC and 10% void cases, depends on the initial loading, and ranges from 350 to greater than 600 GWd/tonne. This is in contrast to the  $\text{UO}_2$  and MOX cases, which retain a Doppler coefficient at least as negative as  $-2.4 \text{ pcm}/^\circ\text{C}$  for the entire duration of their irradiation. Smaller, yet still negative, Doppler coefficients have advantages and disadvantages. The primary advantage is a lower reactivity swing from cold to hot full power conditions, which translates into a less demanding reactivity hold-down requirement. Disadvantages may include poorer response to reactivity-initiated transients, such as a rod ejection or coolant soluble boron dilution. Also, the uncertainty bands of very small negative Doppler coefficients could extend beyond zero into positive values.

Soluble boron worth calculations showed that the boron efficiency of the TRU-only FCM fuel was intermediate between the  $\text{UO}_2$  and MOX cases. This is because although there is only TRU in the fuel, the spectrum is not as hard as in the case of the MOX fuel because of the very low HM loading. Consequently, the observed trend is that lower HM loading (through lower PF or kernel diameter) results in larger negative soluble boron worth. With burnup, the spectrum softens to a more thermal one than that of the  $\text{UO}_2$  case, and so the soluble boron worth becomes quite large and negative. Therefore, soluble boron worth is not expected to be a significant design challenge for the TRU-only FCM fuel. Furthermore, control rod worth is not expected to be a significant issue with this fuel, though calculations at least at an assembly level should be used to verify this.

The analysis of the reactivity effects of 100% voiding suggests that the behavior of this fuel would be similar to MOX fuels of very high plutonium fractions, which are known to have positive void reactivity. In this extensive, though still preliminary, assessment, no soluble or burnable poisons were used and no optimization of spectral effects has been attempted. The optimal balance of moderation, burnable poison loading and locations and soluble boron concentrations has yet to be explored. With the poisons in place in future lattice calculations at the assembly level, the void reactivity calculated will be more realistic. Further analysis should be performed at the assembly and whole core level in order to determine the void reactivity performance of the FCM fuel with such poisons in place.

Loading of TRU-only FCM fuel into an LWR pin without significant quantities of uranium constitutes a challenge to the reactor design from the standpoint of several key reactivity parameters, particularly void reactivity, and to a significant degree the Doppler coefficient. These unit cells, while providing an indication of how a whole core of similar fuel would behave, also provide information of how individual pins of TRU-only FCM fuel would influence the reactivity behavior of a heterogeneous assembly, which was also analyzed in this work.

The plutonium destruction performance of the TRU-only FCM fuel pins is attractive from the standpoint of effectiveness (i.e., the fraction of plutonium that is destroyed). This is a result of the absence of uranium and consequent inability to produce more plutonium as irradiation takes place. The amount of TRU that one may load in the FCM fuel is, however, relatively small compared to ordinary MOX fuel.

### *Heterogeneous Assembly Calculations*

It was also demonstrated that if FCM fuel pins are included in a heterogeneous assembly alongside LEU fuel pins, the overall reactivity behavior is dominated by the uranium pins while attractive TRU destruction performance levels in the TRU-only FCM fuel pins may be preserved. Assembly calculations were performed on various heterogeneous FCM/ $\text{UO}_2$  assembly configurations. Overall, loadings of these types show promise from the standpoint of the reactivity-limited burnup and reactivity coefficients examined. However, some issues remain outstanding that should be examined in future work. These include control rod worth in heterogeneous FCM/ $\text{UO}_2$  assembly configurations and more detailed thermal analysis of the TRU-only FCM fuel pins. It should be noted that the fast fluence values calculated in this work are quite high and exceed the region where data exists to supply the PASTA models. Further investigation should be devoted to more reliable modeling in this regime along with schemes for reduction of fast fluence.

## CONTENTS

ACKNOWLEDGEMENTS .....	v
SUMMARY .....	vii
ACRONYMS .....	xiii
1. INTRODUCTION .....	1
2. OBJECTIVES.....	1
3. METHODOLOGY .....	2
3.1 TRU-Only FCM Fuel Description .....	2
3.2 MOX and UO <sub>2</sub> Fuel Descriptions .....	4
3.3 Code and Methods Used .....	4
3.3.1 Neutronics Calculations.....	4
3.4 Estimation of Fuel Temperatures .....	5
4. RESULTS OF UNIT CELL CALCULATIONS.....	7
4.1 UO <sub>2</sub> and MOX Calculation Results .....	7
4.2 Effects of Packing Fraction and Kernel Size without BP .....	10
4.2.1 Variation of Kernel Size .....	10
4.2.2 Variation of Packing Fraction.....	14
4.2.3 TRISO Particle Fuel Distribution Effect .....	16
4.3 Burnable Poison Effects – Er <sub>2</sub> O <sub>3</sub> .....	18
4.4 Preliminary Analysis of Complete Coolant Voiding .....	20
4.5 Nuclide Inventories .....	22
5. RESULTS OF ASSEMBLY CALCULATIONS.....	23
5.1 Heterogeneous Assemblies Analyzed .....	23
5.2 Results of Assembly Calculations.....	25
5.2.1 Pin Powers .....	25
5.2.2 Reactivity-Limited Burnup and Coefficients.....	34
5.3 Analysis of Complete Coolant Voiding .....	40
5.4 Fast Neutron Fluence .....	40
6. CONCLUSIONS AND FUTURE WORK.....	41
7. REFERENCES .....	44

## LIST OF FIGURES

Figure 4-1. $K_{\infty}$ versus burnup in EFPD and GWd/tonne for UO <sub>2</sub> and MOX unit cells. ....	8
Figure 4-2. MTC versus burnup for UO <sub>2</sub> and MOX unit cells.....	9
Figure 4-3. Void coefficient versus burnup for UO <sub>2</sub> and MOX unit cells using 10% void.....	9

Figure 4-4. Doppler coefficient versus burnup for UO <sub>2</sub> and MOX unit cells.....	9
Figure 4-5. Soluble boron worth versus burnup for UO <sub>2</sub> and MOX unit cells. ....	10
Figure 4-6. K <sub>∞</sub> versus burnup for TRU-only FCM fuel with PF of 48%.....	11
Figure 4-7. MTC versus burnup for TRU-only FCM fuel with various kernel sizes and constant PF.....	11
Figure 4-8. Void coefficient versus burnup for TRU-only FCM fuel with various kernel sizes.....	12
Figure 4-9. Doppler coefficient versus burnup for TRU-only FCM fuel with various kernel sizes.....	12
Figure 4-10. Soluble boron worth versus burnup for TRU-only FCM fuel with various kernel sizes.....	13
Figure 4-11. Neutron spectrum for fresh unit cells of UO <sub>2</sub> , MOX, and FCM. ....	13
Figure 4-12. Neutron spectrum for unit cells of UO <sub>2</sub> , MOX, and FCM, each at approximately end of life.....	14
Figure 4-13. K <sub>∞</sub> versus burnup for TRU-only FCM fuel with kernel diameter of 500 μm. ....	14
Figure 4-14. MTC versus burnup for TRU-only FCM fuel with various PF values. ....	15
Figure 4-15. Void coefficient versus burnup for TRU-only FCM fuel with various PF values. ....	15
Figure 4-16. Doppler coefficient versus burnup for TRU-only FCM fuel with various PF values.....	15
Figure 4-17. Soluble boron worth versus burnup for TRU-only FCM fuel with various PF values. ....	16
Figure 4-18. K <sub>∞</sub> versus burnup for TRU-only FCM fuel with constant fuel loading.....	16
Figure 4-19. MTC versus burnup for TRU-only FCM fuel with constant fuel loading. ....	17
Figure 4-20. Void coefficient versus burnup for TRU-only FCM fuel with constant fuel loading.....	17
Figure 4-21. Doppler coefficient versus burnup for TRU-only FCM fuel with constant fuel loading. ....	17
Figure 4-22. Soluble boron worth versus burnup for TRU-only FCM fuel with constant fuel loading. ....	18
Figure 4-23. K <sub>∞</sub> versus burnup for TRU-only FCM fuel with various Er <sub>2</sub> O <sub>3</sub> contents.....	19
Figure 4-24. MTC versus burnup for TRU-only FCM fuel with range of Er <sub>2</sub> O <sub>3</sub> contents.....	19
Figure 4-25. Void coefficient versus burnup for TRU-only FCM fuel with range of Er <sub>2</sub> O <sub>3</sub> contents.....	19
Figure 4-26. Doppler coefficient versus burnup for TRU-only FCM fuel with range of Er <sub>2</sub> O <sub>3</sub> contents.....	20
Figure 4-27. Soluble boron worth versus burnup for TRU-only FCM fuel with range of Er <sub>2</sub> O <sub>3</sub> contents.....	20
Figure 4-28. Reactivity versus fraction of nominal coolant density for various unit cells.....	21
Figure 4-29. Reactivity versus fraction of nominal coolant density for FCM fuel 500 μm kernel and various Er <sub>2</sub> O <sub>3</sub> loadings.....	22
Figure 5-1. Arrangements of enriched UO <sub>2</sub> and TRU-only FCM pins in heterogeneous PWR assemblies.....	24
Figure 5-2. Diagram of fuel assembly showing the octant reported in subsequent pin power plots. ....	25

Figure 5-3. Relative pin powers at four points during irradiation for the UO <sub>2</sub> -only fuel assembly. ....	26
Figure 5-4. Relative pin powers at four points during irradiation for the MOX fuel assembly. ....	27
Figure 5-5. Relative pin powers at four points during irradiation for FCM configuration 1. ....	28
Figure 5-6. Relative pin powers at four points during irradiation for FCM configuration 2. ....	29
Figure 5-7. Relative pin powers at four points during irradiation for FCM configuration 3. ....	30
Figure 5-8. Relative pin powers at four points during irradiation for FCM configuration 4. ....	31
Figure 5-9. Relative pin powers at four points during irradiation for FCM configuration 5. ....	32
Figure 5-10. Relative pin powers at four points during irradiation for FCM configuration 6. ....	33
Figure 5-11. Relative pin powers at four points during irradiation for FCM configuration 7. ....	34
Figure 5-12. $K_{\infty}$ versus burnup in GWd/tonne for UO <sub>2</sub> , MOX, and heterogeneous FCM/UO <sub>2</sub> assembly configurations. ....	35
Figure 5-14. MTC versus burnup for UO <sub>2</sub> , MOX, and three heterogeneous FCM/UO <sub>2</sub> assembly configurations. ....	36
Figure 5-15. MTC versus burnup for four heterogeneous FCM/UO <sub>2</sub> assembly configurations. ....	36
Figure 5-16. Void coefficient versus burnup for UO <sub>2</sub> , MOX, and three heterogeneous FCM/UO <sub>2</sub> assembly configurations. ....	37
Figure 5-17. Void coefficient versus burnup for four heterogeneous FCM/UO <sub>2</sub> assembly configurations. ....	37
Figure 5-18. Doppler coefficient versus burnup for UO <sub>2</sub> , MOX, and three heterogeneous FCM/UO <sub>2</sub> assembly configurations. ....	38
Figure 5-19. Doppler coefficient versus burnup four heterogeneous FCM/UO <sub>2</sub> assembly configurations. ....	38
Figure 5-20. Soluble boron worth versus burnup for UO <sub>2</sub> , MOX, and three heterogeneous FCM/UO <sub>2</sub> assembly configurations. ....	39
Figure 5-21. Soluble boron worth versus burnup for four heterogeneous FCM/UO <sub>2</sub> assembly configurations. ....	39
Figure 5-22. Reactivity versus fraction of nominal coolant density for four heterogeneous UO <sub>2</sub> /FCM assembly configurations. ....	40
Figure 5-23. Fast fluence (>100 keV) versus burnup for the 6 FCM pin types in assembly configuration 2. ....	41

## LIST OF TABLES

Table 3-1. TRISO fuel particle dimensions and physical properties in FCM fuel. ....	2
Table 3-2. Heavy metal nuclide weight percents in TRU-Ox fuel from spent LWR fuel at 50 MWd/kg burnup. ....	3
Table 3-3. Characteristics of LWR assembly and core initially analyzed. ....	3
Table 3-4. Heavy metal nuclide weight percents in 10% Pu MOX fuel. ....	4
Table 4-1. Heavy metal nuclide consumption (in g/pin) for FCM fuel at various burnup levels. ....	23

## ACRONYMS

BOI	Beginning of Irradiation
CONFU	COmbined Non-Fertile and UO <sub>2</sub>
DB-LWR	Deep Burn Light Water Reactor
EFPD	Effective Full Power Days
EPR	European Pressurized water Reactor
FCM	Fully Ceramic Micro-encapsulated
GWd	Gigawatt-days
HM	Heavy Metal
IMF	Inert Matrix Fuel
LEU	Low-Enriched Uranium
LWR	Light Water Reactor
MOX	Mixed Oxide
MTC	Moderator Temperature Coefficient
PF	Packing Fraction
PWR	Pressurized Water Reactor
TRISO	Tri-isotropic
TRU	Transuranic
TRU-O <sub>x</sub>	Transuranic Oxide
UO <sub>2</sub>	Uranium dioxide



# **NEUTRONIC PERFORMANCE OF TRASURANIC-LOADED FULLY CERAMIC MICRO-ENCAPSULATED FUEL IN LWRs:**

## **FINAL REPORT, INCLUDING VOID REACTIVITY EVALUATION**

### **1. INTRODUCTION**

Over the past few years, the Deep Burn project has evaluated the prospect of using high temperature reactors (HTRs) for reducing legacy inventories of transuranic (TRU) isotopes from used light water reactor (LWR) fuel.<sup>1</sup> This reduction is to be achieved by transmuting the undesirable isotopes, primarily through fissioning or “burning” them. Both pebble bed<sup>2</sup> and prismatic designs<sup>3</sup> were conceptualized and significant design and analysis were performed on them. At present, the focus of the Deep Burn Project has shifted to a once-through burning of the TRU materials in modified LWRs. The subject modification of the LWRs pertains primarily to the form of the fuel to be used. The new fuel form under consideration for use in the Deep Burn LWRs (DB-LWR) is Fully-Ceramic Micro-encapsulated (FCM) fuel, a concept that borrows the tri-isotropic (TRISO) fuel particle design from high-temperature reactor technology.<sup>4</sup> In the DB-LWR concept, these fuel particles would be pressed into compacts using SiC as the matrix material and would be loaded into fuel pins for use in conventional or latter-generation LWRs. The TRU loading is assumed to come from the used fuel of a conventional LWR cooled for 5 years following discharge cooling.

As is the case with Mixed Oxide (MOX) or Inert Matrix Fuel (IMF) concepts, the presence of significant quantities of plutonium and other TRU isotopes alters the reactor physics behavior of LWR cores. Because the TRU-only FCM fuel is meant to contain no significant quantities of uranium, it is likely that neutronically it will most closely resemble the fertile-free IMF.<sup>5</sup> Heterogeneous assemblies containing both uranium pins and fertile-free FCM pins may be necessary to meet reactivity control requirements. These may resemble the COmbined Non-Fertile and UO<sub>2</sub> (CONFU) concepts, which have been studied previously.<sup>6,7</sup> Some initial evaluation of heterogeneous assemblies which combine TRU-only FCM fuel pins alongside UO<sub>2</sub> pins is presented in this work.

### **2. OBJECTIVES**

In order to begin assessing the neutronics characteristics of the TRU-only FCM fuel, unit cell calculations were performed. These unit cell calculations can provide information about the neutronic characteristics of a whole core of similar fuel. Then, assembly calculations were performed evaluating the performance of heterogeneous arrangements of TRU-only FCM fuel pins along with UO<sub>2</sub> pins.

The main objective of this report is to give results of the following activities:

- Evaluate reactivity-limited burnup of TRU-only FCM fuel cells in a Pressurized Water Reactor (PWR)
- Calculate key reactivity coefficients, including total coolant void coefficient, of the TRU-only FCM fuel at various levels of depletion and evaluate the effects of varying the kernel size and packing fraction (PF) on these coefficients
- Compare these results to reference UO<sub>2</sub> and MOX unit cells
- Perform similar calculations on heterogeneous FCM/UO<sub>2</sub> assembly configurations, evaluating reactivity-limited burnup and reactivity coefficients.

A companion report related to another Deep Burn Project milestone [B. Boer et al FCR&D-2011-000338 or INL/EXT-11-23313, presents the results of an evaluation of FCM fuel integrity with depletion levels similar to those investigated in the present report. That other report uses the PASTA code to assess the fuel



performance under steady state conditions (including depletion) as well as under the conditions induced by a simulated LOCA transient.

### 3. METHODOLOGY

Section 3.1 presents information about the assumptions made regarding the design of TRU-only FCM fuel compacts and the LWR assembly into which said fuel is assumed to be loaded. Section 3.2 provides details of the  $\text{UO}_2$  and MOX fuels analyzed as reference cases. In Section 3.3, information is given describing the lattice code and the solution methods used.

#### 3.1 TRU-Only FCM Fuel Description

The specifications chosen for initial analysis approximate the lattice of the AREVA EPR<sup>TM</sup> in part because this reactor is expected to be available in configurations that can accept a core of 100% MOX. Initial calculations were performed by assuming that the ordinary  $\text{UO}_2$  fuel pellets are replaced with the FCM fuel compacts. FCM fuel is constituted of TRISO fuel particles containing TRU- $\text{O}_x$  kernels embedded within a SiC matrix. Table 3-1 shows the dimensions and densities (i.e., specific mass) of the layers of the TRISO particles specified for these initial calculations. The simplifying assumption was made that the kernel diameter can be varied without changing the layer thicknesses, notwithstanding the material integrity implications. Preliminary fuel performance calculations have also been performed to predict the *material* integrity of the TRISO particles constituents of the FCM fuel. Those calculations, using the PASTA code,<sup>8</sup> are the subject of a companion report [B. Boer et al FCR&D-2011-000338 or INL/EXT-11-23313].

Table 3-1. TRISO fuel particle dimensions and physical properties in FCM fuel.

Layer	Thickness ( $\mu\text{m}$ )	Density ( $\text{g/cm}^3$ )
Kernel (TRU- $\text{O}_x$ + SiC)	350–600 <sup>a</sup>	10.0 <sup>b</sup>
Porous Carbon Buffer	100	1.05
Inner Pyrolytic Carbon	35	1.9
SiC	35	3.18
Outer Pyrolytic Carbon	40	1.9

The TRU- $\text{O}_x$  fuel contains primarily neptunium and plutonium with trace amounts of uranium, the vector of which is derived from once-burned LWR fuel. The plutonium oxide is slightly sub-stoichiometric while neptunium and uranium are not. The TRU- $\text{O}_x$  fuel stoichiometry and composition are:

0.2 w/o (nat.  $\text{UO}_2$ ) + 99.8 w/o ( $\text{NpO}_2$  +  $\text{PuO}_{1.8}$ ) + SiC kernel getter

SiC is mixed into the kernel as an oxygen getter. For the purpose of this document, the SiC volume fraction is given and then the remaining kernel space available is filled with TRU- $\text{O}_x$  having density of  $10.0 \text{ g/cm}^3$ . Therefore, the actual kernel density is lower than the value shown in Table 3-1. Nominally, the SiC kernel getter is assumed to take up 25% of the kernel by volume. This composition is adopted from previous studies of Deep Burn High Temperature Reactors.<sup>9</sup> Table 3-2 gives the weight percents of heavy metal nuclides in the FCM fuel.

a. This is the kernel diameter in  $\mu\text{m}$ . This parameter is varied in the analysis within the bounds shown.

b. Density of kernel shown is TRU- $\text{O}_x$  component only. Dilution with SiC ( $\rho = 3.18 \text{ g/cm}^3$ ) reduces total kernel density.

Table 3-2. Heavy metal nuclide weight percents in TRU-Ox fuel from spent LWR fuel at 50 MWd/kg burnup.

Nuclide	Weight Percent
U-235	0.0014
U-238	0.20
Np-237	4.94
Pu-238	3.00
Pu-239	58.11
Pu-240	21.97
Pu-241	5.18
Pu-242	6.60

Table 3-3 gives parameters for the reactor design assumed in this stage of the study. As mentioned above, the basic parameters are taken from the AREVA EPR<sup>TM</sup> design.<sup>10</sup> The assumed power rating is 4500 MW<sub>th</sub> and the number of 17x17 fuel assemblies was 241. In order to model the FCM fuel at this initial stage of analysis, the oxide fuel ordinarily used in an EPR is simply replaced with fuel compacts of the type described above having and TRISO particle packing fractions of  $\leq 48\%$ , which has been estimated to be the maximum feasible without causing excessive failures.<sup>11</sup> The cladding is Zircalloy-4 with a mass density of 6.56 g/cm<sup>3</sup>. For the single pin cell calculations, an effective pin pitch of 1.32 cm is used in order to account for the extra water in the empty guide tubes and in the small inter-assembly gap. These same dimensions are used in the assembly calculations presented in Section 5 as well with the exception of the use of the actual pin pitch rather than the effective one.

Table 3-3. Characteristics of LWR assembly and core initially analyzed.

Parameter	Value
Reactor thermal power (MW <sub>th</sub> )	4500
Number of Fuel Assemblies	241
Active Fuel Height (m)	4.20
Assembly Pitch (cm)	21.504
Actual Pin Pitch (cm)	1.27
Effective pin pitch for single cell calculations (cm)	1.32
Number of fueled pins per 17 × 17 assembly	265
Number of guide tubes per 17 × 17 assembly	24
Fuel Pellet Diameter (mm)	8.20
Fuel Pin Inner Diameter (mm)	8.36
Fuel Pin Outer Diameter (mm)	9.50
Guide Tube Inner Diameter (mm)	11.4
Guide Tube Outer Diameter (mm)	12.3
Average Linear Power (kW/m)	16.7
Average Power per Volume of Core (MW <sub>th</sub> /m <sup>3</sup> )	96.2
Average Power per Volume of Fuel Pellet (W/cm <sup>3</sup> )	318

## 3.2 MOX and UO<sub>2</sub> Fuel Descriptions

Unit cells similar to that of the FCM fuel described above containing conventional LWR fuels are also analyzed as reference cases. The two selected cases are an enriched UO<sub>2</sub> cell and a MOX cell. The UO<sub>2</sub> case assumes a fuel density of 10.4 g/cm<sup>3</sup> and an enrichment of 4.5 w/o <sup>235</sup>U. The MOX fuel is assumed to have a density of 10.0 g/cm<sup>3</sup> and 10 w/o plutonium with the balance of the heavy metal being representative of tails uranium having 0.3 w/o <sup>235</sup>U. Table 3-4 shows the heavy metal nuclide weight percents in the 10% Pu MOX fuel cell that is analyzed. These values represent a prediction of the average of the once-burned LWR plutonium available in France in 2015.<sup>12</sup> The French design is selected for this case because of data and specifications availability in the open literature.

The assumed assembly and unit cell dimensions are identical to those of the FCM fuel described in Section 3.1. The volumetric power density is also the same as for the FCM fuel, which leads to a much lower specific power since the heavy metal loading is much higher in UO<sub>2</sub> and MOX fuel than in the FCM fuel. As with the FCM fuel, an effective pin pitch of 1.32 cm is used in the cell calculations to account for additional water in guide tubes and in inter-assembly gaps.

Assembly based-calculations presented in Chapter 5 use TRU-only FCM fuel along with conventional UO<sub>2</sub> pins. These UO<sub>2</sub> pins have an enrichment of 4.3 w/o.

Table 3-4. Heavy metal nuclide weight percents in 10% Pu MOX fuel.

Nuclide	Weight Percent
Uranium	90
U-235	0.3
U-238	99.7
Plutonium	10
Pu-238	2.7
Pu-239	56.0
Pu-240	25.9
Pu-241	7.4
Pu-242	7.3
Am-241	0.7

## 3.3 Code and Methods Used

### 3.3.1 Neutronics Calculations

Calculations were performed using DRAGON-4, an open-source lattice transport code developed and maintained by École Polytechnique de Montréal.<sup>13</sup> This code contains multiple solution methods and allows for flexible calculation routes and data manipulation. The code also allows for treatment of the double-heterogeneity of the TRISO particles in the fuel directly using the method developed by Hébert.<sup>14</sup> Collision probability calculations were performed using a cross section library generated from ENDF/B-VII and cast in the SHEM-281 energy group structure.<sup>15</sup>

In LWR analysis, calculations on a single unit cell can be informative with regard to the performance of a certain fuel in the whole core. As a first step, the TRU-only FCM fuel was analyzed as a single unit cell as though it was the only fuel type present in the core. The results are interpreted with the knowledge that if the TRU-only pin were used in conjunction with UO<sub>2</sub> pins or assemblies, the overall behavior would be

expected to be the composite result of the effects of the TRU-only FCM unit cells and the  $\text{UO}_2$  unit cells. This was verified in subsequent calculations on full heterogeneous assemblies.

Each type of fuel investigated is depleted based on a flux calculation using a  $B_0$  buckling search in order to correct the spectrum. At each depletion step, several perturbations on the unit cell are performed for calculation of the various reactivity coefficients. The parameters calculated at each burnup step in each case are:

- Moderator Temperature Coefficient (MTC) – This is calculated by increasing the water coolant temperature by  $5^\circ\text{C}$  and adjusting the density accordingly from  $0.714 \text{ g/cm}^3$  to  $0.702 \text{ g/cm}^3$ . Results are reported in pcm/ $^\circ\text{C}$ . This is performed without soluble boron in the coolant. With the addition of enough soluble boron to make the reactor critical, the MTC would be diminished. This calculation, however, allows comparison to the  $\text{UO}_2$  and MOX reference cases on a consistent basis.
- Void Coefficient (10% void) – This is calculated by decreasing the water coolant density by 10% and recalculating the flux, again with a  $B_0$  buckling search. This is again carried out without soluble boron in the coolant. Results are reported in pcm/% void.
- Doppler Coefficient – This is calculated by increasing the temperature of the fuel by  $50^\circ\text{C}$  and recalculating the flux. In the case of the solid pellet fuel (MOX and  $\text{UO}_2$  cases) along with the homogenized FCM fuel case, there is only one temperature used in the fuel. In the case of the FCM fuel with doubly heterogeneous details, the problem is simplified by setting all temperatures in the TRISO particles and SiC matrix to the same temperature. The Doppler coefficient is thus calculated by raising all temperatures simultaneously. This simplification should be abandoned in later work as more sophisticated heat transfer models are integrated into the calculations.
- Soluble Boron Worth – This is calculated by adding 1000 ppm of natural boron (19.9 %  $^{10}\text{B}$  by mass) to the coolant and recalculating flux. Results are presented in pcm/ppm.

In all cases, reactivity differences in pcm are calculated by taking the difference in  $k_\infty$  divided by the nominal  $k_\infty$ , or:

$$\frac{k_{\infty, \text{pert}} - k_{\infty, \text{nom}}}{k_{\infty, \text{nom}}} \quad (1)$$

Where  $k_{\infty, \text{pert}}$  is the perturbed  $k_\infty$  (e.g., high temperature, partially-voided condition, 1000 ppm boron) and  $k_{\infty, \text{nom}}$  is the nominal  $k_\infty$ . In all of these calculations (except soluble boron worth), no soluble boron is assumed.

The analysis of complete (or nearly complete) voiding in unit cells presented in Section 4.4 used a slightly different methodology. A buckling search was not used, but rather a fixed buckling based on the size of an EPR core and the Eigenvalue without leakage ( $k^*$ ) was reported. These analyses were performed at beginning of irradiation and the coolant density was varied from nominal down to 1% of nominal.

### 3.4 Estimation of Fuel Temperatures

Thermal calculations were performed in order to provide an approximation of nominal fuel temperatures as input to the lattice code. The methodology and assumptions used for this are described in the following paragraphs.

The unirradiated (phonon) conductivity of SiC in unit of  $\text{W} \cdot \text{m}^{-1} \cdot \text{K}^{-1}$  as a function of the temperature [K] can be described with the following correlation (for  $T > 300\text{K}$ ), (for a “Highly pure and dense single-/poly-crystals” case):<sup>16</sup>

$$K_{\text{non,irr}} = \left( -3.0 \times 10^{-4} + 1.05 \times 10^{-5} T \right)^{-1} \quad (2)$$

At room temperature this correlation gives a conductivity of  $350 \text{ W} \cdot \text{m}^{-1} \cdot \text{K}^{-1}$ . Neutron radiation introduces defects in the SiC material resulting in an increase of the thermal resistance ( $1/K_{\text{rd}}$ ). The conductivity of irradiated SiC can then be described by:

$$K_{\text{irr}} = \left( \frac{1}{K_{\text{non,irr}}} + \frac{1}{K_{\text{rd}}} \right)^{-1} \quad (3)$$

The thermal resistance ( $1/K_{\text{rd}}$ ) due to radiation at a temperature range of  $750 - 850^\circ\text{C}$  is 0.031 and 0.040 at fast ( $E > 0.1 \text{ MeV}$ ) neutron fluence levels of  $1.0 \times 10^{21}$  and  $5.0 \times 10^{21} \text{ n/cm}^2$ , respectively. These correlations result in thermal conductivity values between 20 and  $25 \text{ W} \cdot \text{m}^{-1} \cdot \text{K}^{-1}$  for these temperatures and fluence levels.

The temperature in a fuel pin with dispersed coated fuel particles can be estimated from the pin power density and the temperature at the pin outer boundary. For the effective conductivity of a fuel pin ( $K_{\text{eff}}$ ) a Maxwell-Garnett model is adopted<sup>17</sup>, which takes into account both the coated particles and the SiC matrix:

$$K_{\text{eff}} = \lambda_m \left( \frac{\lambda_i(1+2\alpha) - \lambda_m(2\alpha-2)}{\lambda_m(2+\alpha) + \lambda_i(1-\alpha)} \right) \quad (4)$$

where  $\lambda_i$  is the conductivity of the fuel kernel,  $\lambda_m$  is the conductivity of the SiC matrix and  $\alpha$  is the volume fraction of fuel kernels in the matrix. It is assumed that the coating layers of the particle, consisting of SiC and carbon, have roughly the same conductivity of the SiC matrix. It is noted that with a packing fraction of 50 % of coated particles in the fuel pin and the radii of the kernel and coated particle (kernel and coating layers) at  $175 \mu\text{m}$  and  $390 \mu\text{m}$ , respectively,  $\alpha$  takes the value 0.045. Assuming that the kernel has a conductivity of  $2 \text{ W} \cdot \text{m}^{-1} \cdot \text{K}^{-1}$  and the SiC matrix a conductivity of  $20 \text{ W} \cdot \text{m}^{-1} \cdot \text{K}^{-1}$ , there results an effective conductivity for the fuel pin of  $18 \text{ W} \cdot \text{m}^{-1} \cdot \text{K}^{-1}$ .

The temperature drop across the fuel pin can be calculated with:

$$\Delta T_{\text{fuel}} = \frac{q'}{4\pi K_{\text{eff}}} \quad (5)$$

With a linear power,  $q'$ , of  $500 \text{ W/cm}$ , a temperature drop of  $221 \text{ K}$  is found. This is small compared to the typical temperature drop in a “normal”  $\text{UO}_2$  fuel pellet or pin at this linear power, which is around  $1400 \text{ K}$ . The temperature drop over the gap, Zr-cladding and coolant at this power are  $200 \text{ K}$ ,  $80 \text{ K}$  and  $20 \text{ K}$ , respectively (for example see Ref. 18). At a typical coolant temperature of  $580 \text{ K}$  the LWR-DB fuel centerline temperature is  $1200 \text{ K}$ . Note that a linear power of  $500 \text{ W/cm}$  is a conservative value, since the average linear power in an EPR type reactor of  $4500 \text{ MW}_{\text{th}}$  is approximately  $170 \text{ W/cm}$ . The latter linear power would result in a center fuel temperature of  $791 \text{ K}$ .

The temperature difference between the center and the outer surface of the fuel kernel is given by:

$$\Delta T_{\text{ker } n} = \frac{q_{\text{ker } n}^m R_{\text{ker } n}^2}{6K_{\text{ker } n}} \quad (6)$$

in which  $q'''$  is volumetric power,  $R$  is radius, and the subscript *kern* refers to the kernel properties. Assuming a power density and a thermal conductivity, respectively, of  $7.0 \text{ GW/m}^3$  and  $2 \text{ W}\cdot\text{m}^{-1}\cdot\text{K}^{-1}$  for the kernel leads to a temperature difference of 18 K. The temperature difference over the gap can be calculated with:<sup>19</sup>

$$\Delta T_{gap} = \frac{q'''_{kern} R_{kern}^3}{3K_{gap}} \left( \frac{1}{R_{buf,0} - t_{gap}} - \frac{1}{R_{buf,0}} \right) \quad (7)$$

where  $K_{gap}$  is the effective gap thermal conductivity and  $R_{buf}$  is the outer radius of the buffer layer. The gap radius ( $t_{gap}$ ) in this equation is calculated from the volume change of the buffer with:<sup>19</sup>

$$t_{gap} = R_{buf,0} - \sqrt[3]{R_{kern}^3 + \frac{(1 + \Delta V)V_{buf,0}}{4/3\pi}} \quad (8)$$

where  $V_{buf}$  is the initial buffer volume and  $\Delta V$  is the change in buffer volume. A gap thickness of  $18 \text{ }\mu\text{m}$  is found, assuming that the buffer volume decreases by 25%. This leads to a temperature difference over the gap (with  $K_{gap} = 3.2 \times 10^{-2} \text{ W}\cdot\text{m}^{-1}\cdot\text{K}^{-1}$  (see ref. [20])) of 102 K. The average kernel centerline temperature at the pin center can therefore be expected to be around 900 K. This temperature was used as the nominal temperature in all fuel as a simplifying assumption, but it is suspected that cooler temperatures in the FCM fuel than in traditional  $\text{UO}_2$  or MOX may create some additional design margin with respect to certain accident scenarios. However, further analysis of this is warranted in order to reach definitive conclusions.

## 4. RESULTS OF UNIT CELL CALCULATIONS

This section presents the results of the unit cell calculations, beginning with those from the  $\text{UO}_2$  and MOX unit cells. These are then used as a basis for comparison with the TRU-only FCM fuel cases to be studied in the remainder of Section 4.

### 4.1 $\text{UO}_2$ and MOX Calculation Results

This section reports on the examination of unit cells of  $\text{UO}_2$  and MOX. For each of these, the behavior of the key reactivity coefficients is presented as burnup proceeds. Both enriched  $\text{UO}_2$  cores and partial MOX cores have accumulated many years of operational experience in addition to being licensed in multiple countries. While they are not yet in use, 100% MOX cores have been demonstrated theoretically to be feasible in EPRs,<sup>21</sup> albeit with some minor changes to the design and to the mode of operation. By drawing comparisons to the performance of these types of fuels, the feasibility of the TRU-only FCM fuel can be assessed.

Figure 4-1 shows  $k_\infty$  versus burnup in Effective Full Power Days (EFPD) and GWd/tonne for the unit cells described in Section 3.2 and containing  $\text{UO}_2$  and MOX. The first reactivity coefficient examined in this comparison is the MTC. The values for this coefficient do not differ significantly between the MOX and  $\text{UO}_2$  fresh fuel cases, and both become more negative during depletion aside from a small turnaround in the case of  $\text{UO}_2$  at just beyond 40 GWd/tonne. Void coefficients of reactivity calculated using 10% void are shown in Figure 4-3. These too are similar in the  $\text{UO}_2$  and MOX cases and remain negative throughout burnup.

Figure 4-4 shows the Doppler coefficient versus burnup for the  $\text{UO}_2$  and MOX unit cells. The Doppler coefficient for MOX fuel is more negative than that of  $\text{UO}_2$  at beginning of irradiation (BOI); however, with depletion, as plutonium is bred in it, the  $\text{UO}_2$  fuel experiences a decrease of its Doppler coefficient which becomes very similar to that of MOX; the latter's Doppler coefficient rises slightly with depletion. The

conjunction of these changes results in the Doppler coefficients for both types of fuel to be within a narrow band of one another at burnup levels between 30 and 40 GWd/tonne. One disadvantage of the more negative Doppler coefficient in MOX is that more cold shutdown worth is required as the change in reactivity from cold shutdown to hot full power conditions is greater than in the  $\text{UO}_2$  case. However, the  $\text{UO}_2$  experiences a similar disadvantage at higher burnup levels, which in turn implies the necessity of a control rod design that is capable of similar cold shutdown reactivity hold down.

Figure 4-5 shows the reactivity worth of soluble boron in the coolant versus burnup for  $\text{UO}_2$  and MOX unit cells. Because MOX fuel has a harder neutron spectrum than the  $\text{UO}_2$  fuel, the (spectrum weighted) effective absorption cross section of boron is smaller in the MOX case. In a partial MOX core, this is not a major concern because, as with other reactivity coefficients, the whole-core effects are due to the combined influences of the  $\text{UO}_2$  and MOX cells that constitute it. In the case of a 100% MOX core, this low soluble boron worth would be considered unacceptable and boric acid enriched in  $^{10}\text{B}$  has been proposed for use as chemical shim.<sup>21</sup> A limit of soluble boron efficiency equal to (or more negative than) -4 pcm/ppm has been proposed in previous work.<sup>12</sup>

In core designs containing 100% MOX assemblies, an increase in the moderator/fuel ratio has been proposed to mitigate the poor reactivity feedback and control worth characteristics of the core, for example by replacing fuel rods with water holes or by increasing fuel rod diameters. This has been shown to extend the burnup and increase plutonium consumption while increasing the effectiveness of control materials and improving various other reactivity coefficients.<sup>21,22,23,24,25</sup>

Not analyzed here, but also very important in quantifying the safety performance of an LWR core, is the reactivity effect of completely voided coolant channels. This is discussed separately for both the  $\text{UO}_2$  and FCM unit cell cases in Section 4.4.

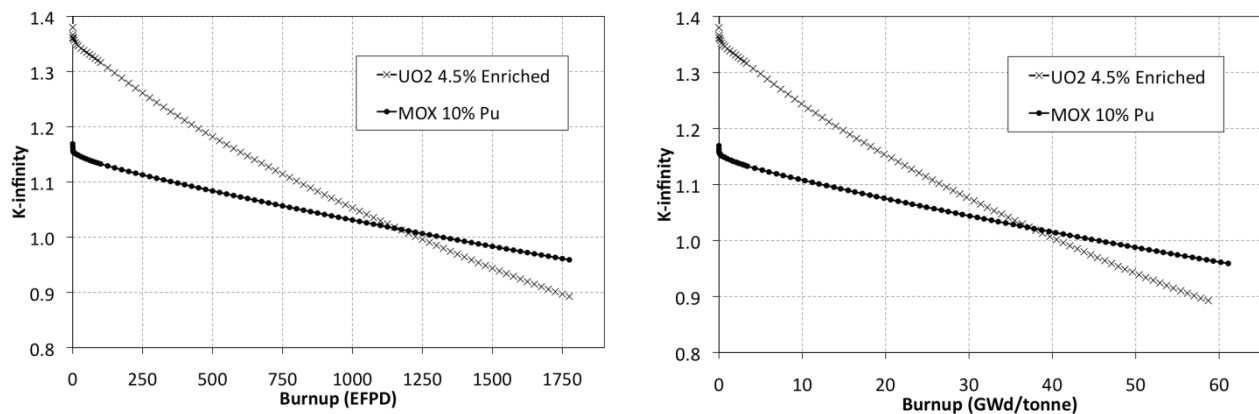


Figure 4-1.  $K_{\infty}$  versus burnup in EFPD and GWd/tonne for  $\text{UO}_2$  and MOX unit cells.



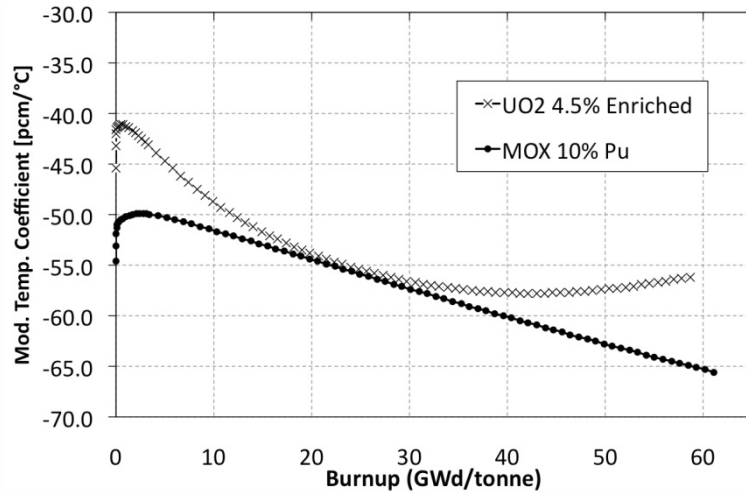


Figure 4-2. MTC versus burnup for UO<sub>2</sub> and MOX unit cells.

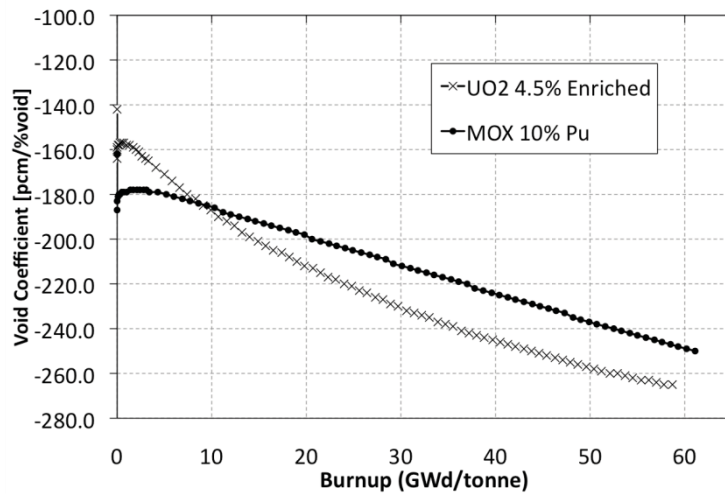


Figure 4-3. Void coefficient versus burnup for UO<sub>2</sub> and MOX unit cells using 10% void.

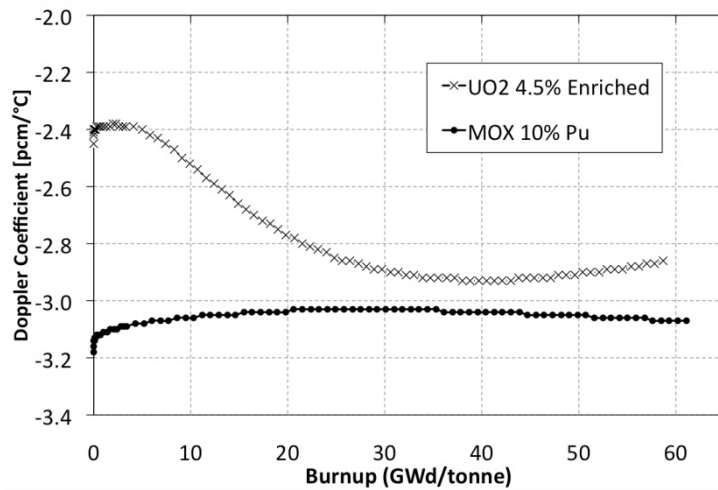


Figure 4-4. Doppler coefficient versus burnup for UO<sub>2</sub> and MOX unit cells.



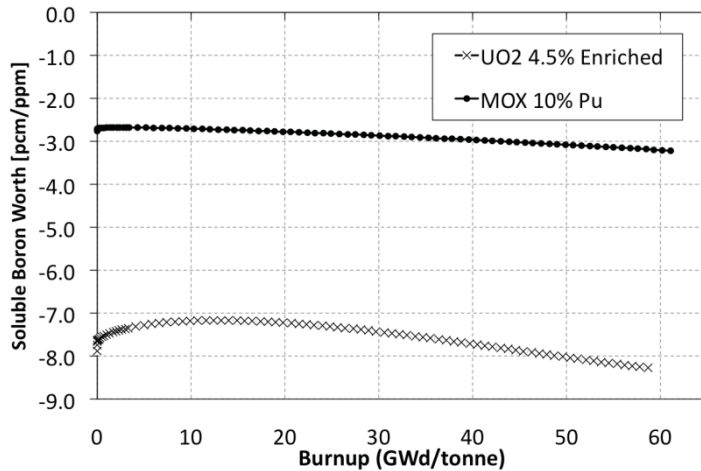


Figure 4-5. Soluble boron worth versus burnup for UO<sub>2</sub> and MOX unit cells.

## 4.2 Effects of Packing Fraction and Kernel Size without BP

### 4.2.1 Variation of Kernel Size

In this section, the effects of varying the kernel size on the various reactivity coefficients are analyzed. The analyses are performed while keeping constant the PF at 48% and varying kernel diameter. Two key simplifying assumptions are made for this analysis: the temperatures are unchanged in the fuel with changes in kernel size, and that the buffer thickness of 100  $\mu\text{m}$  is sufficient for all cases. Because the buffer is carbon, which is found also in the TRISO particle layers and in the SiC matrix, its thickness is *a-priori* expected to have a minimal impact on the neutronics behavior (although a later study may be needed to assess the ultimate validity of this assumption). However, given a particular PF and kernel diameter, the buffer thickness can impact the fuel loading and its capacity to contain fission product gases needs attention.

Figure 4-6 shows  $k_{\infty}$  versus burnup for TRU-only FCM fuel with a PF of 48%. Three different kernel sizes are shown, 400, 500 and 600  $\mu\text{m}$  diameters. These correspond to effective plutonium densities in the fuel compact of 0.37, 0.51, and 0.65  $\text{g}/\text{cm}^3$ , respectively. Compared to the 10% Pu MOX value of 0.88  $\text{g}/\text{cm}^3$  plutonium, all of these are small. Furthermore, the 600  $\mu\text{m}$  diameter kernel case may represent a very optimistically large fuel loading for the configurations under consideration. This variation in the plutonium loading between these three FCM cases is the primary reason for the vast differences in the behavior of  $k_{\infty}$  versus burnup (in EFPD) shown on the left in Figure 4-6. Since the volumetric power is the same in each case, different loadings change the specific power ( $\text{W}/\text{g HM}$ ) significantly.

The reactivity limited burnup of the FCM unit cells in general appears to be short compared to that of UO<sub>2</sub> and MOX. In the UO<sub>2</sub> and MOX cases,  $k_{\infty}$  crosses 1.0 around 1200 EFPD, whereas this occurs in the TRU-only FCM fuel at between 400 and 800 EFPD. Depending on the acceptable kernel dimensions from a fuel performance standpoint, the length of time which the TRU-only FCM fuel could sustain criticality at this power density appears to be quite short due to the low heavy metal (HM) capacity of the fuel form. This may be a factor in determining whether a core consisting of 100% TRU-only FCM fuel should be pursued without even considering the challenges from a safety standpoint, which will be addressed later. In a heterogeneous assembly, low enriched uranium (LEU) could be used to drive the TRU-only FCM pins to high burnup levels and perhaps a more attractive cycle length would result. This hypothesis was verified in work presented in Section 5.

Figure 4-7 shows the MTC versus burnup for each of the kernel sizes. Each case starts in the -20 to -30  $\text{pcm}/^{\circ}\text{C}$  range and after a slow increase in negative magnitude, begins to turn upward towards zero. The

case with the smallest amount of fuel (400  $\mu\text{m}$  diameter kernel) exhibits a positive MTC around 500 GWd/tonne. This is because so little HM remains that the system has become overmoderated (and an increase in temperature implies a decrease in density with the concomitant decrease in moderation). Other cases become positive later, at higher burnup levels. The likelihood of reaching such high levels of burnup is low. Later studies, at the assembly and full core levels, will be necessary to determine the actual values of MTC with the eventual mix of soluble and burnable poisons to be used. The same can be said of the void coefficient assuming 10% void, which is shown in Figure 4-8. Again, the trend here is that the fuel type with the smallest loading (400  $\mu\text{m}$  diameter kernel) has the least negative feedback value and turns positive before the other kernel sizes.

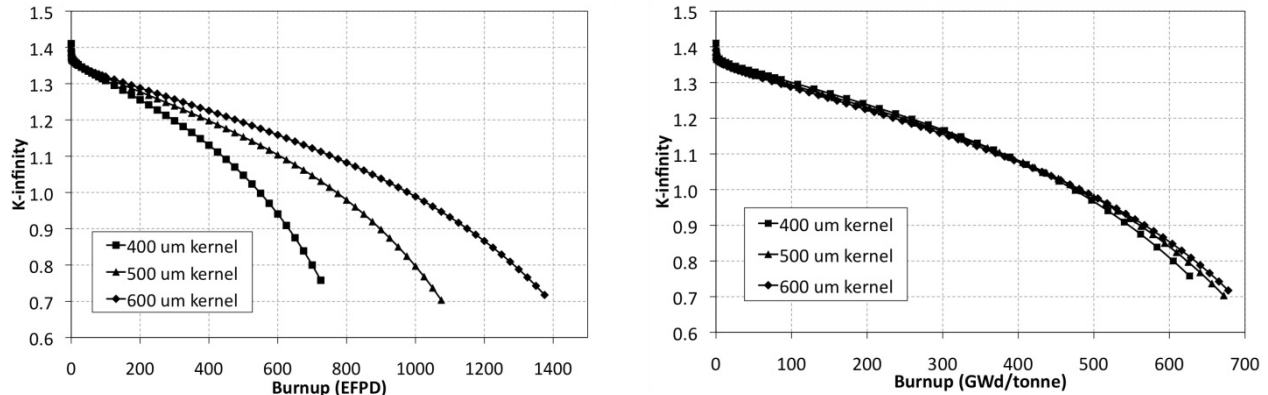


Figure 4-6.  $K_{\infty}$  versus burnup for TRU-only FCM fuel with PF of 48%.

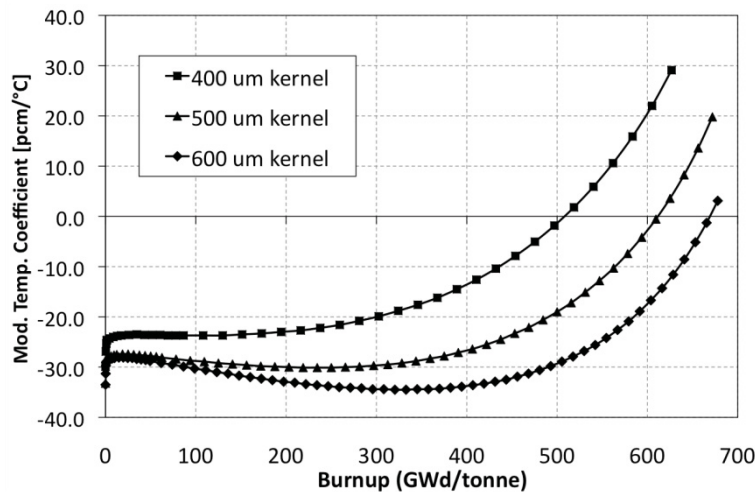


Figure 4-7. MTC versus burnup for TRU-only FCM fuel with various kernel sizes and constant PF.

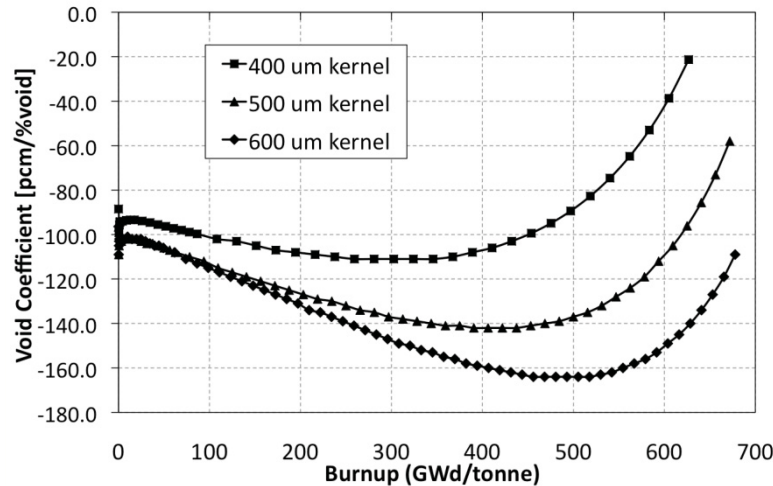


Figure 4-8. Void coefficient versus burnup for TRU-only FCM fuel with various kernel sizes.

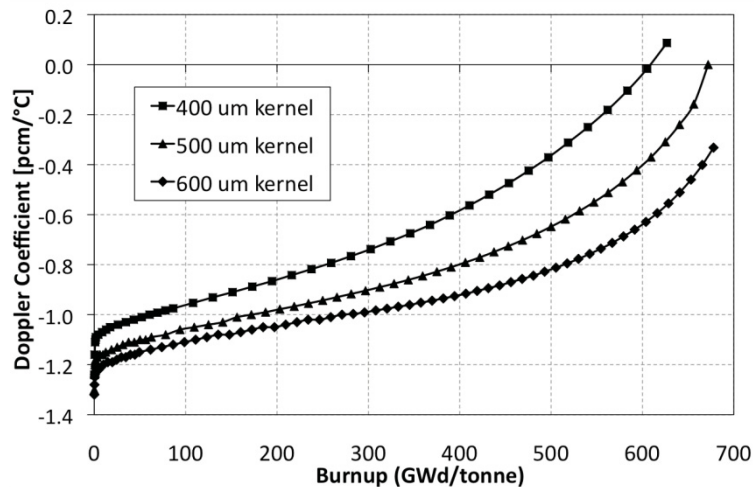


Figure 4-9. Doppler coefficient versus burnup for TRU-only FCM fuel with various kernel sizes.

Figure 4-9 shows the Doppler coefficient versus burnup for TRU-only FCM fuel with various kernel sizes and a fixed PF of 48%. In all of three of these cases, the BOI value is around -1.2 pcm/°C. With increasing burnup, the magnitude for all of these cases decreases until 0 is reached at >600 GWd/tonne. This is in contrast to the UO<sub>2</sub> and MOX cases, which remain at least as negative as -2.0 pcm/°C for the duration of their irradiation. Smaller, yet still negative, Doppler coefficients have advantages and disadvantages. The primary advantage is a lower Doppler-induced reactivity swing from cold to hot full power conditions, which translates to less additional reactivity shutdown hold-down required. Disadvantages include more severe response to reactivity-initiated transients, such as a rod ejection or boric acid dilution. Also, the uncertainty bands of very small negative Doppler coefficients can extend beyond zero into positive values. While it is true that this coefficient should be analyzed carefully in the design of this type of system, if heterogeneous assemblies containing mostly uranium are used, the Doppler coefficient will be made substantially more negative and this problem may be rendered moot.

Figure 4-10 shows soluble boron worth as a function of burnup for the three cases analyzed here, again all assuming a constant PF of 48%. The fresh fuel values of the soluble boron reactivity worth for these FCM cases are between -4 and -7 pcm/ppm boron. This is intermediate between the UO<sub>2</sub> and MOX cases shown in Figure 4-5. With increased burnup, the boron efficiency of the FCM fuel becomes very negative and

reaches -20 pcm/ppm in the most extreme of the cases shown here. In contrast, the boron efficiency in the MOX and  $\text{UO}_2$  cases is relatively unchanged with depletion. The cause of this can be understood by examining the neutron spectra of the various cases. The small boron efficiency of MOX fuel is a design challenge; ways of overcoming said challenge were mentioned in Section 4.1. The cause of this challenge and the reason it is not a problem in  $\text{UO}_2$  fuel is the very hard neutron spectrum of MOX fuel cells compared to the spectrum of  $\text{UO}_2$  cells. Furthermore, both of these fuel types see a relatively unchanged spectrum during depletion. In the case of FCM fuel, the spectrum at BOI is intermediate to the  $\text{UO}_2$  and MOX cases, leading to intermediate soluble boron efficiency. Figure 4-11 shows the neutron spectra from MOX,  $\text{UO}_2$ , and FCM fueled cells with a kernel diameter of 500  $\mu\text{m}$  at zero burnup, and Figure 4-12 shows the same at roughly the expected discharge burnup values of each fuel type. During depletion, the spectrum in FCM fuel becomes much more thermal than that of the MOX and  $\text{UO}_2$  cases; hence, the very large negative soluble boron worth at later burnup levels.

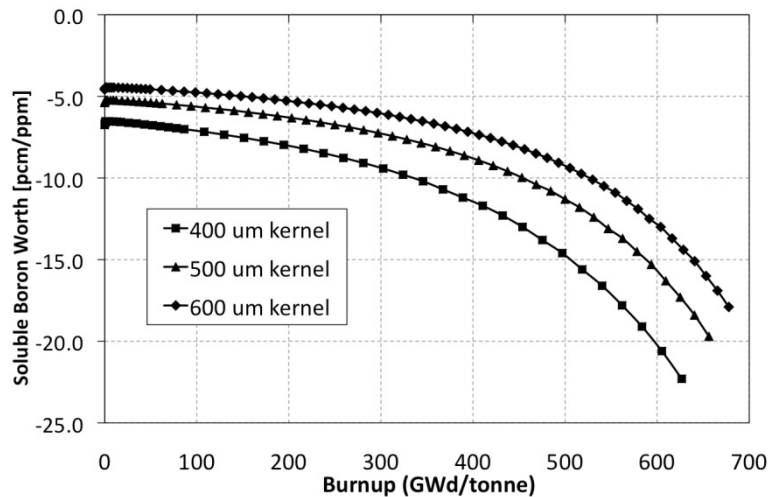


Figure 4-10. Soluble boron worth versus burnup for TRU-only FCM fuel with various kernel sizes.

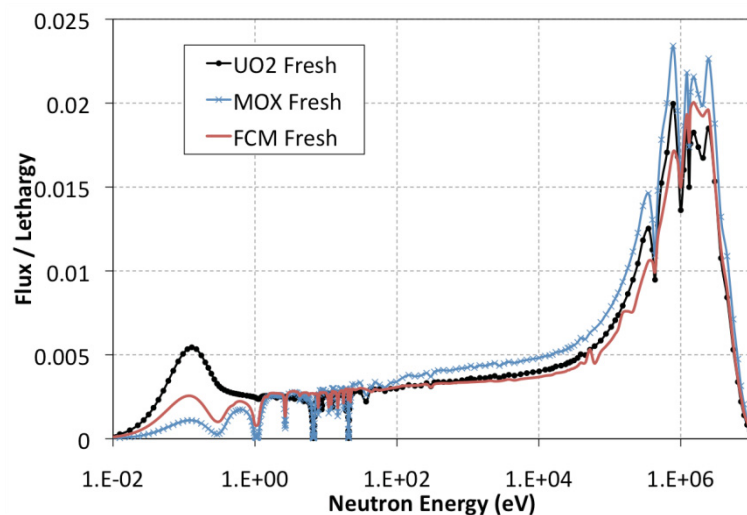


Figure 4-11. Neutron spectrum for fresh unit cells of  $\text{UO}_2$ , MOX, and FCM.

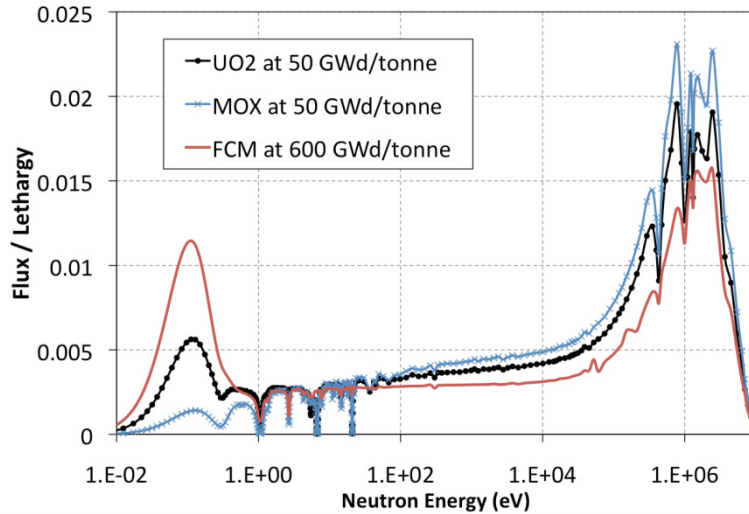


Figure 4-12. Neutron spectrum for unit cells of UO<sub>2</sub>, MOX, and FCM, each at approximately end of life.

#### 4.2.2 Variation of Packing Fraction

This section repeats the analyses from Section 4.2.1, only now the kernel size is fixed at a diameter of 500  $\mu\text{m}$  and the PF is varied incrementally from 20% to 48%. These cases correspond to effective plutonium densities in the compacts of 0.21, 0.32, 0.43, and 0.51  $\text{g}/\text{cm}^3$ , respectively. The results are analogous to those of the study of the variation of kernel diameter with fixed PF, and so they are not discussed here in detail. Note that the fuel loading appears to be the primary driver for the burnup and reactivity coefficient behavior of the unit cells. This will be further analyzed in the following section where the amount of fuel is held constant while simultaneously varying the PF and kernel size.

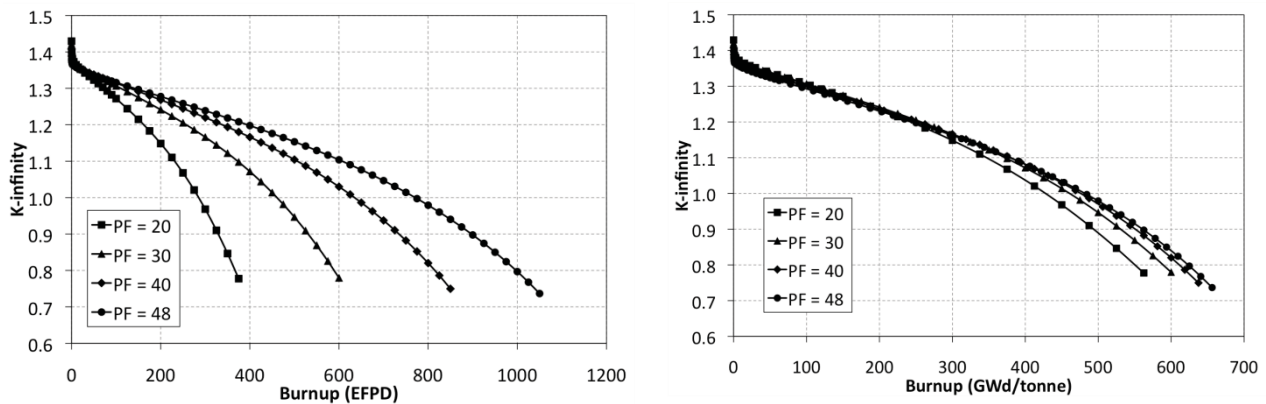


Figure 4-13.  $K_{\infty}$  versus burnup for TRU-only FCM fuel with kernel diameter of 500  $\mu\text{m}$ .

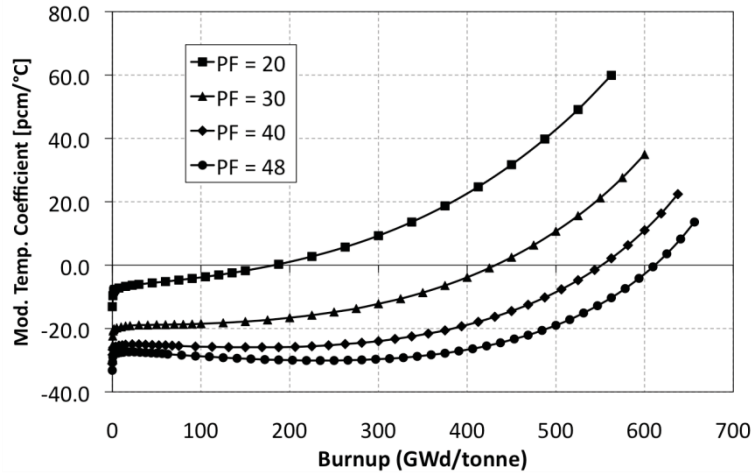


Figure 4-14. MTC versus burnup for TRU-only FCM fuel with various PF values.

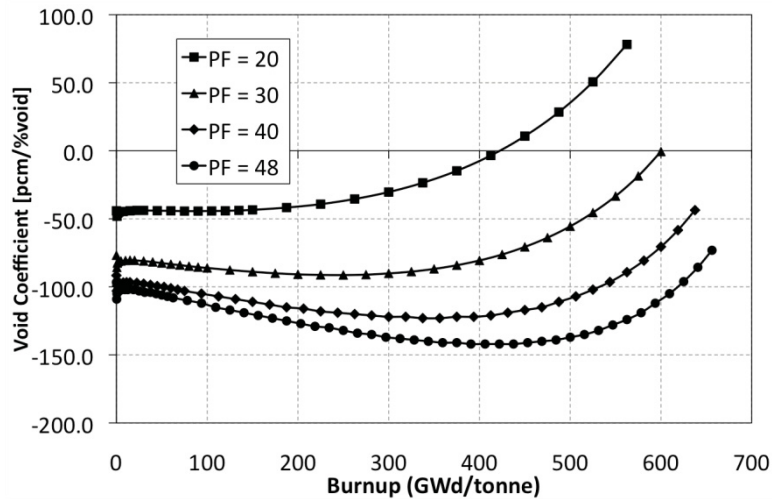


Figure 4-15. Void coefficient versus burnup for TRU-only FCM fuel with various PF values.

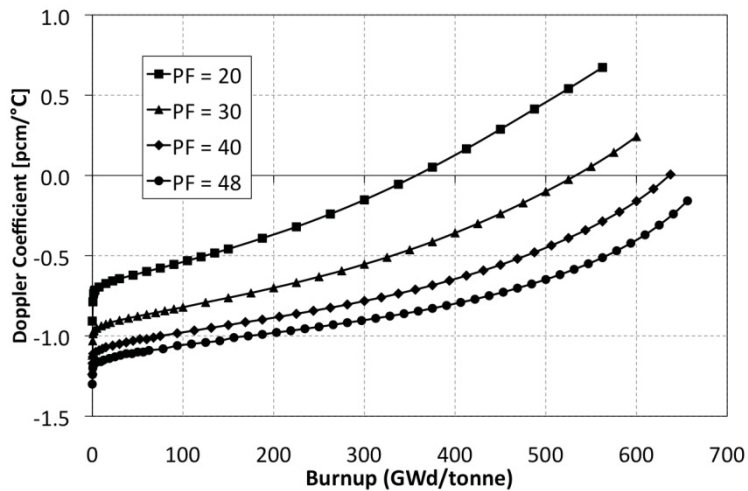


Figure 4-16. Doppler coefficient versus burnup for TRU-only FCM fuel with various PF values.



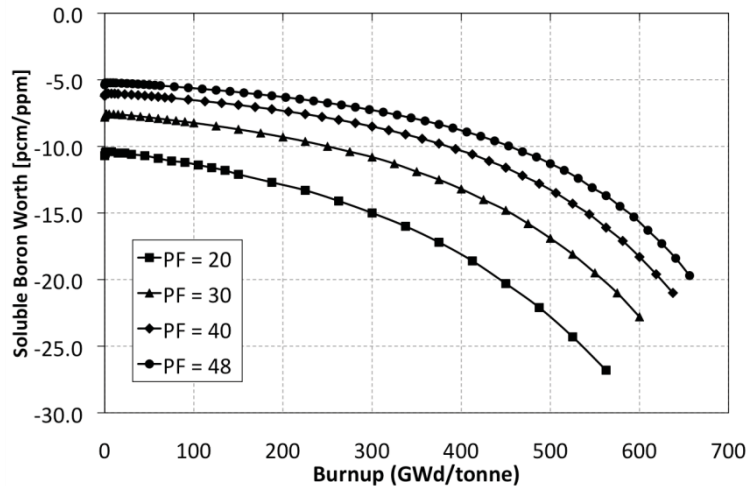


Figure 4-17. Soluble boron worth versus burnup for TRU-only FCM fuel with various PF values.

#### 4.2.3 TRISO Particle Fuel Distribution Effect

To verify that the fuel loading is the primary variable in determining the reactivity coefficient behavior of the TRU-only FCM fuel, cases are analyzed where the amount of fuel is held constant while the PF and kernel diameter are simultaneously varied. A case is also included where the entire fuel compact, matrix and TRISO particles, are homogenized. The effective plutonium density on a per-volume-of-compact basis in the selected case is  $0.30 \text{ g/cm}^3$ . Figure 4-18 shows the reactivity versus burnup for these cases. It is evident that the behavior is not significantly affected by the variation of the kernel size and PF parameters. Figure 4-19 through Figure 4-22 again repeat the coefficients shown in previous sections for the various constant-loading cases. Some variation is observed between the homogenized case and the FCM fuel with microstructures, but very little difference exists between FCM cases of constant fuel and varying kernel diameters. These results confirm that the actual fuel loading is the main driver dictating the reactivity performance of the TRU-only FCM fuel.

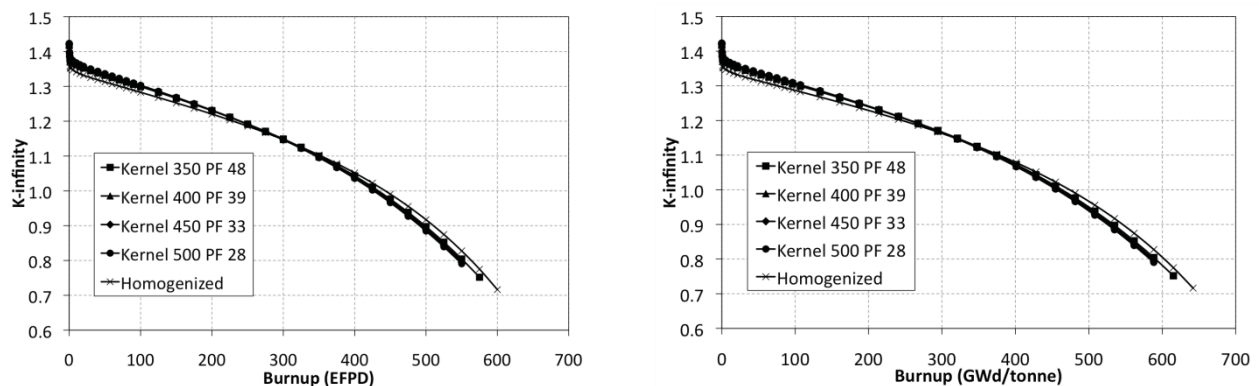


Figure 4-18.  $K_{\infty}$  versus burnup for TRU-only FCM fuel with constant fuel loading.

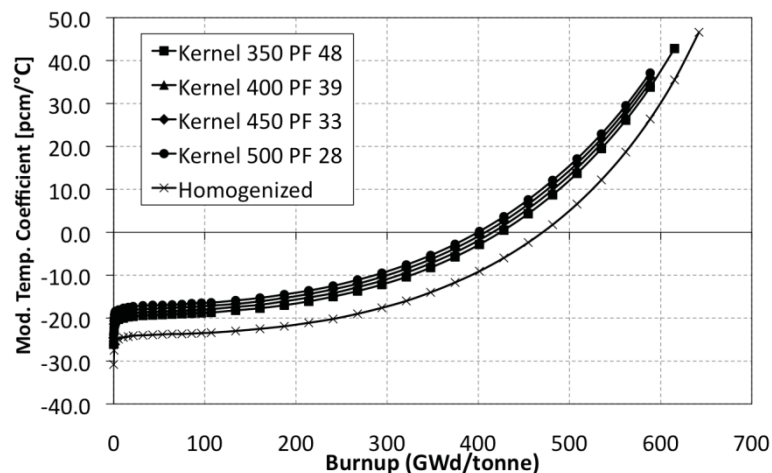


Figure 4-19. MTC versus burnup for TRU-only FCM fuel with constant fuel loading.

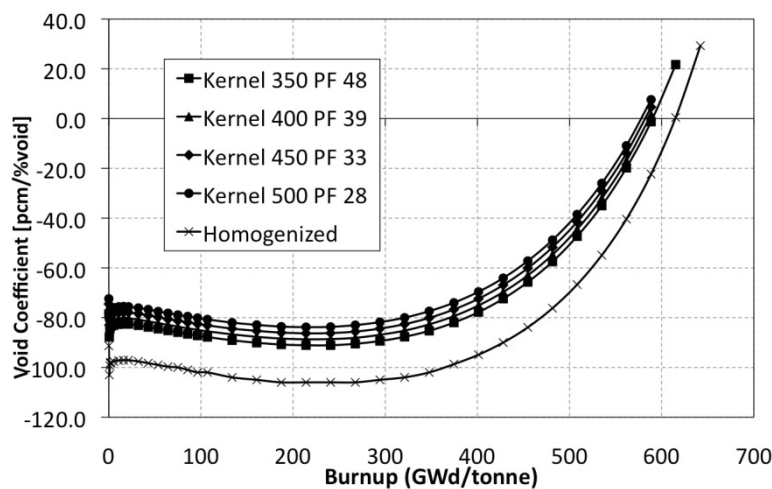


Figure 4-20. Void coefficient versus burnup for TRU-only FCM fuel with constant fuel loading.

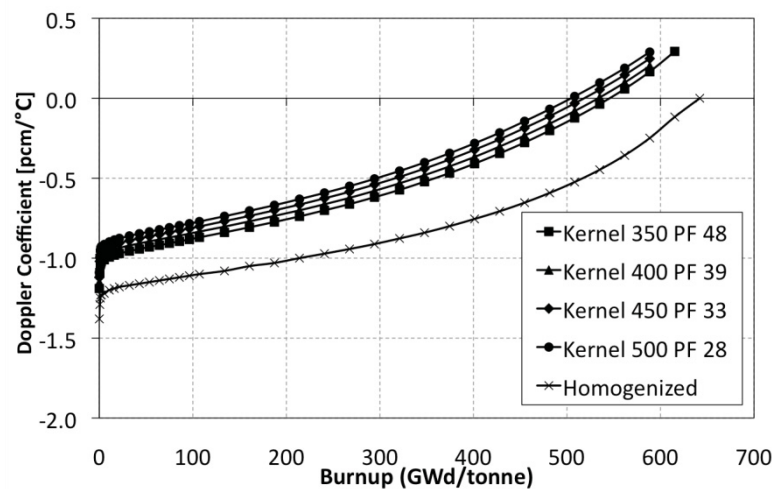


Figure 4-21. Doppler coefficient versus burnup for TRU-only FCM fuel with constant fuel loading.



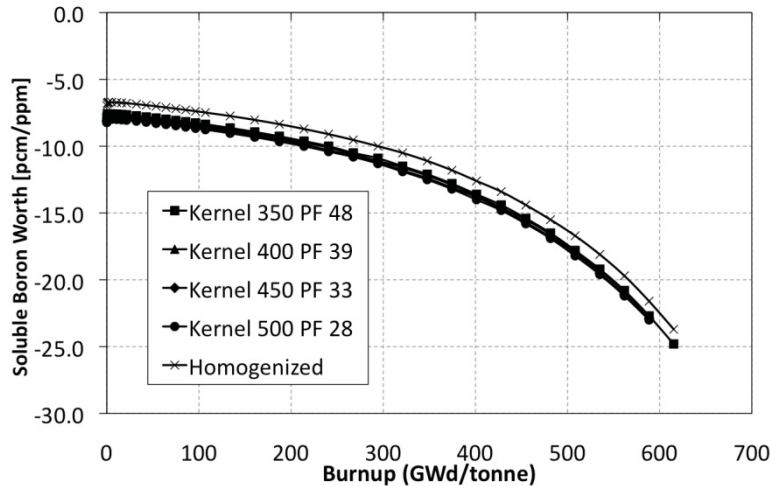


Figure 4-22. Soluble boron worth versus burnup for TRU-only FCM fuel with constant fuel loading.

### 4.3 Burnable Poison Effects – $\text{Er}_2\text{O}_3$

To enhance the safety characteristics of the feedback parameters, previous designers of full-core uranium-free inert matrix fuel (IMF) cores proposed that resonant absorbers be used as burnable poisons. These were shown to mitigate the challenges of uranium-free core loadings, particularly the 100% void reactivity.<sup>26,27,28</sup> As a preliminary assessment of the effects of the more promising burnable poisons on the unit cell neutronic performance, several loadings of  $\text{Er}_2\text{O}_3$  are investigated here. In Figure 4-23 through Figure 4-27, the same parameters as in previous sections are given versus burnup for four different  $\text{Er}_2\text{O}_3$  loadings given in weight percent. A case without  $\text{Er}_2\text{O}_3$  having PF of 48% and kernel diameter of 500  $\mu\text{m}$  is shown. This is then followed by 5, 10, and 20 %  $\text{Er}_2\text{O}_3$  cases with the same kernel dimensions and packing fraction. Note that the weight percent  $\text{Er}_2\text{O}_3$  is calculated not including the 25% by volume occupied by SiC getter within the kernel, which remains constant throughout all the calculations discussed in this report. These cases have effective plutonium loadings of 0.51, 0.48, 0.45, 0.40  $\text{g}/\text{cm}^3$ , respectively. Thus, some of the effects observed as  $\text{Er}_2\text{O}_3$  content increases are due to the absorption by erbium, and some result from simply displacing the fuel.

Figure 4-23 shows  $k_\infty$  versus burnup in EFPD (left) and GWd/tonne (right). The plot against EFPD shows that the reactivity-limited burnup is reduced with increasing  $\text{Er}_2\text{O}_3$  content. However, from the plot against GWd/tonne, one sees that this is not due in large part to residual reactivity loss from erbium absorption, but primarily an effect of displacing TRU from the kernel. Figure 4-24 and Figure 4-25 show MTC and void coefficient (10% void) versus burnup, respectively. Both of these show that increasing  $\text{Er}_2\text{O}_3$  content makes these coefficients more negative. As supported by information in the previous sections, the observation is made that decreasing TRU content tends to make these coefficients less negative. In contrast, the decrease in TRU content that comes from increasing  $\text{Er}_2\text{O}_3$  content is not accompanied by a similar behavior of “less negative” coefficients, instead, as seen in the figures the increase of poison content and concomitant decrease of TRU content are accompanied by an increase in magnitude of the negative coefficients. A competing effect might be present, but it is dwarfed and drowned by the poison effect. It can also be observed from Figure 4-26 and Figure 4-27 that Doppler coefficient and soluble boron efficiency are not to a large degree affected by the  $\text{Er}_2\text{O}_3$  content.

In future studies, heterogeneous assemblies of combinations of TRU-only FCM cells and uranium, the need for burnable poisons, both resonant absorbers and otherwise, should be evaluated. As in the case of MOX fuel, if an acceptable limit on the TRU content of FCM-uranium heterogeneous assemblies is determined, the need for poisons to enhance feedback mechanisms may be obviated. This would be an attractive

outcome, especially from the consequent ability to load more TRU into the TRISO particles of the FCM fuel.

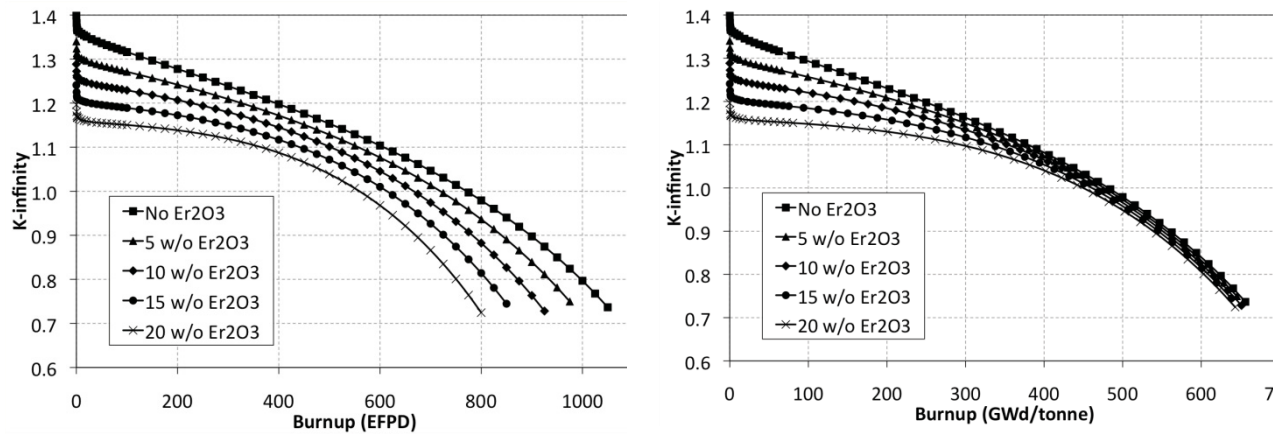


Figure 4-23.  $K_{\infty}$  versus burnup for TRU-only FCM fuel with various  $\text{Er}_2\text{O}_3$  contents.

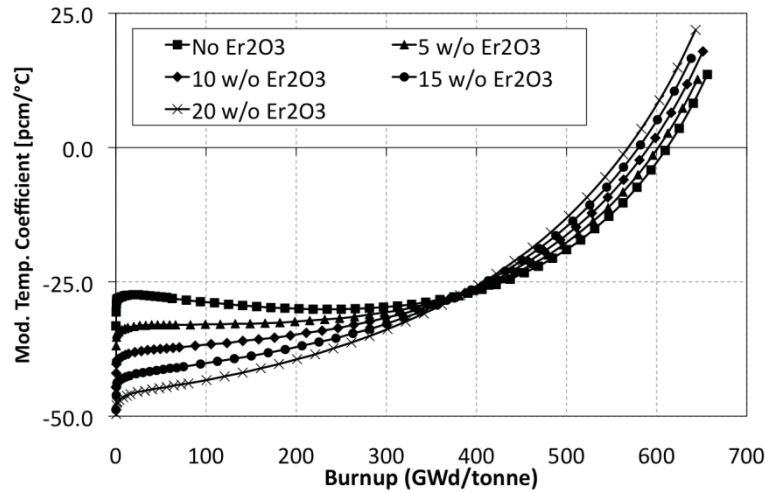


Figure 4-24. MTC versus burnup for TRU-only FCM fuel with range of  $\text{Er}_2\text{O}_3$  contents.

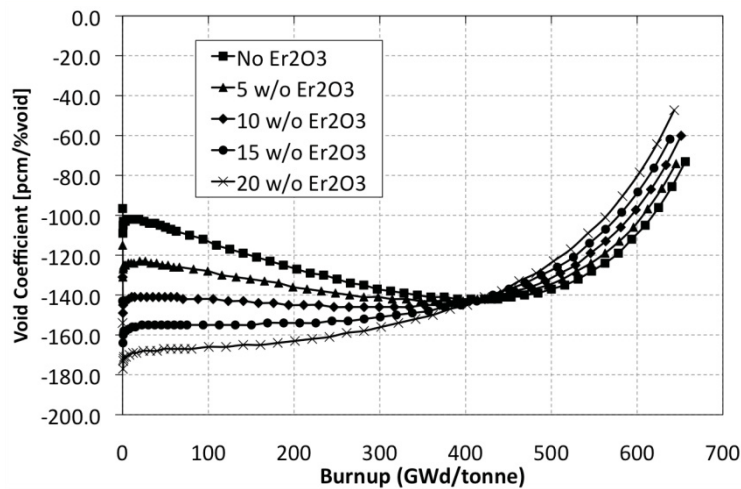


Figure 4-25. Void coefficient versus burnup for TRU-only FCM fuel with range of  $\text{Er}_2\text{O}_3$  contents.

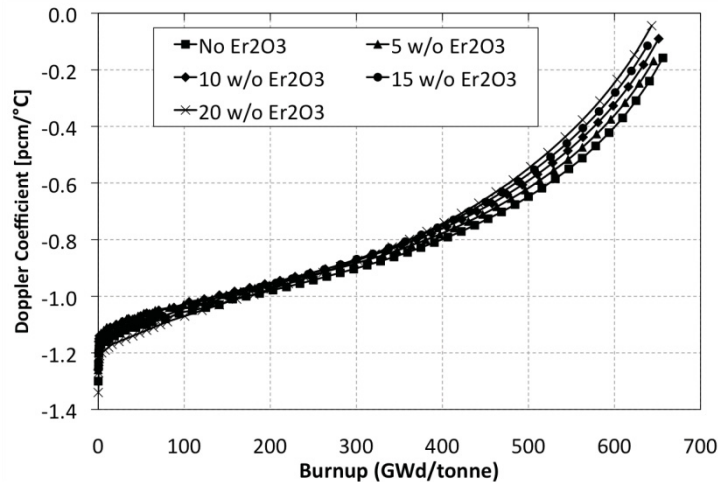


Figure 4-26. Doppler coefficient versus burnup for TRU-only FCM fuel with range of  $\text{Er}_2\text{O}_3$  contents.

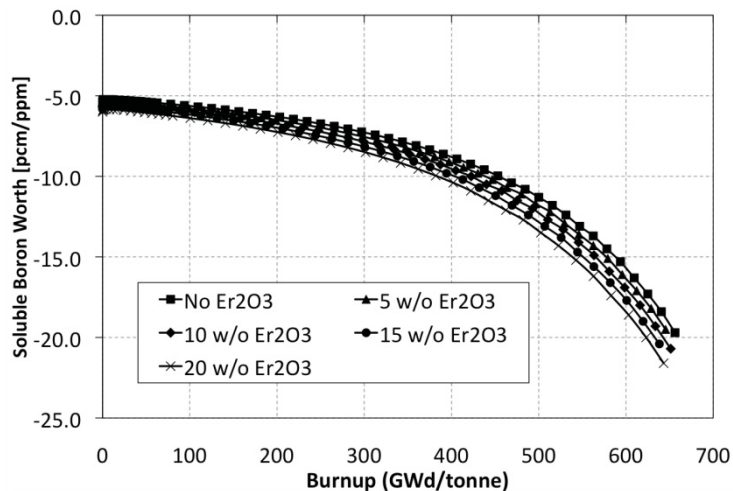


Figure 4-27. Soluble boron worth versus burnup for TRU-only FCM fuel with range of  $\text{Er}_2\text{O}_3$  contents.

#### 4.4 Preliminary Analysis of Complete Coolant Voiding

In low-enriched  $\text{UO}_2$  cores, the voided-core reactivity is low due to the absence of the moderation necessary to the efficient thermalization of neutrons. In the case of MOX, there are competing effects. Voiding the core hardens the neutron spectrum, which causes an increase in resonance absorption in  $^{238}\text{U}$ , but also decreases resonance absorption in  $^{240}\text{Pu}$ .<sup>29</sup> In MOX fuel having greater than ~10–15% Pu, the  $^{240}\text{Pu}$  effect exceeds the  $^{238}\text{U}$  effect and the voided reactivity can be greater than unity. This is the reason for the limit of 12% placed on Pu content of MOX fuel.<sup>30</sup> Since the TRU-only FCM fuel is without  $^{238}\text{U}$ , which would mitigate the  $^{240}\text{Pu}$  related voiding effects; this issue may present a design challenge, possibly necessitating a limit on the fraction of the fuel that may be TRU-only FCM, a consequence analogous to that of the case of MOX.

In this section, the  $\text{UO}_2$  case, the MOX case, and some of the FCM cases are analyzed to examine the effects of various moderator densities on reactivity. For this, a fixed geometric buckling is assumed ( $2.2 \text{ m}^{-2}$ ) and the Eigenvalue without leakage ( $k^*$ ) is plotted. No soluble or burnable poisons are used at this point, as the optimal balance of the two has not yet been explored. With the poisons in place, the void reactivity will look very different. The purpose of this study is only to compare the effects of the different fuels on the

voided reactivity in a consistent manner. More detailed analyses should be performed at the assembly and whole core levels to determine the void reactivity performance of the FCM fuel with these poisons in place.

Figure 4-28 shows reactivity ( $k^*$ ) versus fraction of nominal coolant density for various unit cell types. The  $\text{UO}_2$  curve shows a monotonic decrease in reactivity with decreasing coolant density, whereas the MOX decreases and then increases as the very high void fraction leads to the loss of the effect of the 1-eV neutron resonance absorption reaction in  $^{240}\text{Pu}$ . Three FCM cases are plotted here, each with particle PF of 48%, and with respective kernel sizes of 400, 500, and 600  $\mu\text{m}$  diameters. In these cases, a decrease followed by a rather sharp increase in reactivity occurs as coolant density approaches zero. This is due to the presence of plutonium without the mitigating effects of  $^{238}\text{U}$ . The 600  $\mu\text{m}$  diameter kernel case was then altered by elimination of all the carbon that was present. The observed resulting effect is shown by the white triangles curve in Figure 4-28. Also plotted is the MOX case with all of the uranium removed, shown with white circles. The similarities in these plots illustrate the strong analogous behaviors of the TRU-only FCM fuel and the MOX fuel without the natural uranium and with some carbon added to moderately lower the voided  $k^*$ , as it tends to do in a fast spectrum. This behavior pattern suggests that a limit analogous to the 12% plutonium limit in MOX could be identified for TRU-only FCM fuel that would render and maintain the void reactivity permanently negative.

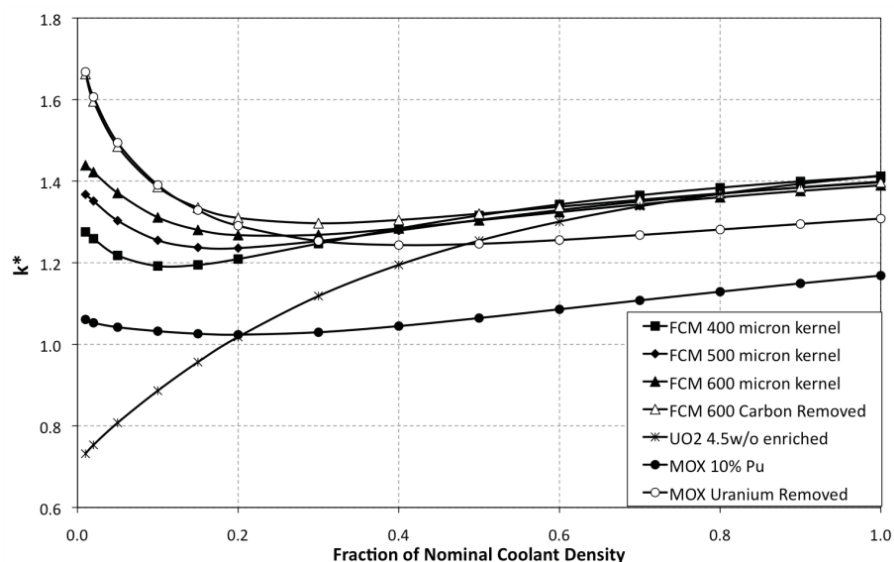


Figure 4-28. Reactivity versus fraction of nominal coolant density for various unit cells.

Figure 4-29 shows the same plot as Figure 4-28, only now it is with all FCM fuel with 500  $\mu\text{m}$  diameter kernels and PF of 48% and with various  $\text{Er}_2\text{O}_3$  loadings given in weight percent. As the weight fraction of  $\text{Er}_2\text{O}_3$  increases, the  $k^*$  values decrease regardless of the moderator density. Some of this effect is from poisoning by erbium, and some is due to simply displacing fuel from the fuel cell. To separate the effects, the erbium atoms were removed from the 20 w/o  $\text{Er}_2\text{O}_3$  case. This is also shown in Figure 4-29. From this plot, one can see that a significant amount of poisoning is from the erbium and not only the displacement of fuel. As before, this only gives some indication of the behavior of the different types of unit cells, and without more realistic assemblies with burnable and soluble poison schemes in place, the void reactivity cannot be definitively known. This should be explored in later work.

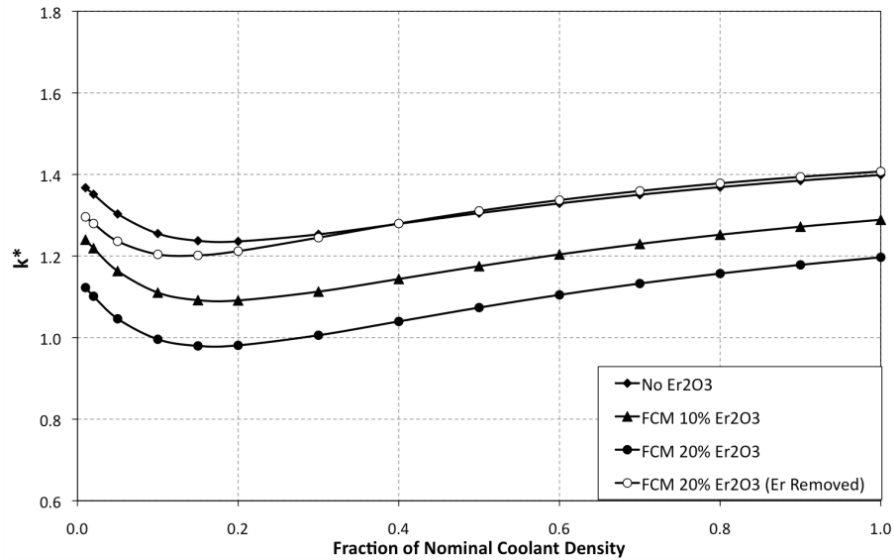


Figure 4-29. Reactivity versus fraction of nominal coolant density for FCM fuel 500  $\mu\text{m}$  kernel and various  $\text{Er}_2\text{O}_3$  loadings.

## 4.5 Nuclide Inventories

To make a preliminary assessment of the TRU destruction performance of the FCM fuel, a case based on using 400  $\mu\text{m}$  diameter kernels and TRISO particle PF of 48% is analyzed further. Heavy metal nuclide quantities in g/pin are given in Table 4-1 for BOI and three different burnup levels: 400, 500, and 600 GWd/tonne. This is done on a per-pin basis because the arrangement of TRU-only FCM fuel pins in the assemblies and core are not yet known.

The total heavy metal present at BOI is 81.8 g/pin, 77.6 of which is plutonium, and 47.5 of which is  $^{239}\text{Pu}$ . Assuming the intermediate discharge burnup of 500 GWd/tonne, the *total* plutonium consumption is 42.8 g/pin, or 55% of the initial plutonium. The  $^{239}\text{Pu}$  *isotopic* consumption at this burnup is 43.2 g/pin, or 91% of the initial  $^{239}\text{Pu}$ . Assuming the more optimistic discharge burnup of 600 GWd/tonne, the *total* plutonium consumption is 51.3 g/pin, or 66% of the initial plutonium. The  $^{239}\text{Pu}$  *isotopic* consumption at this burnup is 46.1 g/pin, or 97% of the initial  $^{239}\text{Pu}$ . No americium is initially loaded, and 1.77 g/pin or 2.04 g/pin is produced at 500 and 600 GWd/tonne, respectively. No curium is initially loaded, and 0.85 g/pin or 1.29 g/pin is produced at 500 and 600 GWd/tonne, respectively.

The plutonium destruction performance of this fuel is attractive from the standpoint of the fraction which is destroyed. This is a result of the absence of uranium and its associated inevitable production of more plutonium with irradiation. The amount of TRU that can be loaded in the FCM fuel is, however, relatively small at 81.8 g/pin. For comparison, in a typical MOX pin having 10 % plutonium, there is approximately 200 g of plutonium loaded.

Table 4-1. Heavy metal nuclide consumption (in g/pin) for FCM fuel at various burnup levels.

Nuclide	BOI	400 GWd/tonne	$\Delta$ 400–0.0 GWd/tonne	500 GWd/tonne	$\Delta$ 500–0.0 GWd/tonne	600 GWd/tonne	$\Delta$ 600–0.0 GWd/tonne
<sup>235</sup> U	1.15E-03	4.34E-03	3.19E-03	5.57E-03	4.42E-03	6.57E-03	5.43E-03
<sup>238</sup> U	1.64E-01	1.46E-01	-1.81E-02	1.40E-01	-2.32E-02	1.35E-01	-2.89E-02
<sup>238</sup> Pu	2.45E+00	2.76E+00	3.03E-01	2.61E+00	1.54E-01	2.23E+00	-2.24E-01
<sup>239</sup> Pu	4.75E+01	9.71E+00	-3.78E+01	4.35E+00	-4.32E+01	1.43E+00	-4.61E+01
<sup>240</sup> Pu	1.80E+01	1.68E+01	-1.13E+00	1.39E+01	-4.02E+00	9.64E+00	-8.33E+00
<sup>241</sup> Pu	4.24E+00	7.38E+00	3.14E+00	6.31E+00	2.08E+00	4.30E+00	6.08E-02
<sup>242</sup> Pu	5.40E+00	6.59E+00	1.19E+00	7.54E+00	2.14E+00	8.72E+00	3.32E+00
<sup>237</sup> Np	4.04E+00	2.59E+00	-1.45E+00	2.19E+00	-1.85E+00	1.73E+00	-2.31E+00
<sup>241</sup> Am	0.00E+00	2.28E-01	2.28E-01	2.11E-01	2.11E-01	1.41E-01	1.41E-01
<sup>242m</sup> Am	0.00E+00	3.23E-03	3.23E-03	2.92E-03	2.92E-03	1.83E-03	1.83E-03
<sup>243</sup> Am	0.00E+00	1.24E+00	1.24E+00	1.55E+00	1.55E+00	1.90E+00	1.90E+00
<sup>242</sup> Cm	0.00E+00	7.54E-02	7.54E-02	1.15E-01	1.15E-01	1.54E-01	1.54E-01
<sup>243</sup> Cm	0.00E+00	1.21E-03	1.21E-03	2.31E-03	2.31E-03	3.74E-03	3.74E-03
<sup>244</sup> Cm	0.00E+00	4.23E-01	4.23E-01	6.83E-01	6.83E-01	1.06E+00	1.06E+00
<sup>245</sup> Cm	0.00E+00	2.44E-02	2.44E-02	4.02E-02	4.02E-02	5.28E-02	5.28E-02
<sup>246</sup> Cm	0.00E+00	1.97E-03	1.97E-03	5.83E-03	5.83E-03	1.53E-02	1.53E-02
<sup>247</sup> Cm	0.00E+00	1.65E-05	1.65E-05	6.13E-05	6.13E-05	1.96E-04	1.96E-04
U Total	1.65E-01	1.50E-01	-1.49E-02	1.46E-01	-1.88E-02	1.41E-01	-2.35E-02
Pu Total	7.76E+01	4.33E+01	-3.43E+01	3.48E+01	-4.28E+01	2.63E+01	-5.13E+01
Np Total	4.04E+00	2.59E+00	-1.45E+00	2.19E+00	-1.85E+00	1.73E+00	-2.31E+00
Am Total	0.00E+00	1.47E+00	1.47E+00	1.77E+00	1.77E+00	2.04E+00	2.04E+00
Cm Total	0.00E+00	5.26E-01	5.26E-01	8.47E-01	8.47E-01	1.29E+00	1.29E+00
HM Total	8.18E+01	4.80E+01	-3.38E+01	3.97E+01	-4.21E+01	3.15E+01	-5.03E+01

## 5. RESULTS OF ASSEMBLY CALCULATIONS

Heterogeneous fuel assembly arrangements were developed and analyzed in DRAGON. This was done in order to test the hypothesis that the neutronics characteristics of the UO<sub>2</sub> and FCM fuel would combine to perform the TRU-burning function of the FCM fuel, yet with neutronics feedback parameters heavily influenced by the UO<sub>2</sub> pins. In all, seven different heterogeneous arrangements of pins were tested along with one all UO<sub>2</sub> assembly and a 12% Pu MOX assembly to serve as reference cases for comparison to the heterogeneous cases. The FCM fuel used in this section is comprised of TRU-only kernels of diameter 500  $\mu$ m with a PF of 44% by volume. This was selected over the 48% value used previously in order to add more conservatism from the standpoint of fuel integrity.

### 5.1 Heterogeneous Assemblies Analyzed

Figure 5-1 shows the seven heterogeneous assembly configurations modeled. Numbers of FCM pins in the various heterogeneous assemblies range from 44 of the available 264 fuel locations (Configuration 1) to 108 of the 264 locations (Configuration 7). Some of the cases locate the TRU-only FCM pins near the periphery of the assembly, as in Configuration 1. Assuming all assemblies in the core are identical (an assumption inherent in the reflected boundary condition), this leads to the FCM fuel experiencing the hardest neutron spectrum. Other cases surround the empty guide tubes with the FCM fuel pins, as in Configurations 2 and 3. Combinations of these two strategies are also included, as in Configuration 5.

For each heterogeneous assembly case, depletion analysis was performed with branching calculations to calculate the reactivity feedback parameters calculated in previous sections at the unit cell level. These



calculations were performed using  $1/8^{\text{th}}$  assembly symmetry and powers are reported in the octant shown in Figure 5-2. In these calculations, each fuel pin was depleted separately in order to track the movement of pin power peaking throughout burnup.

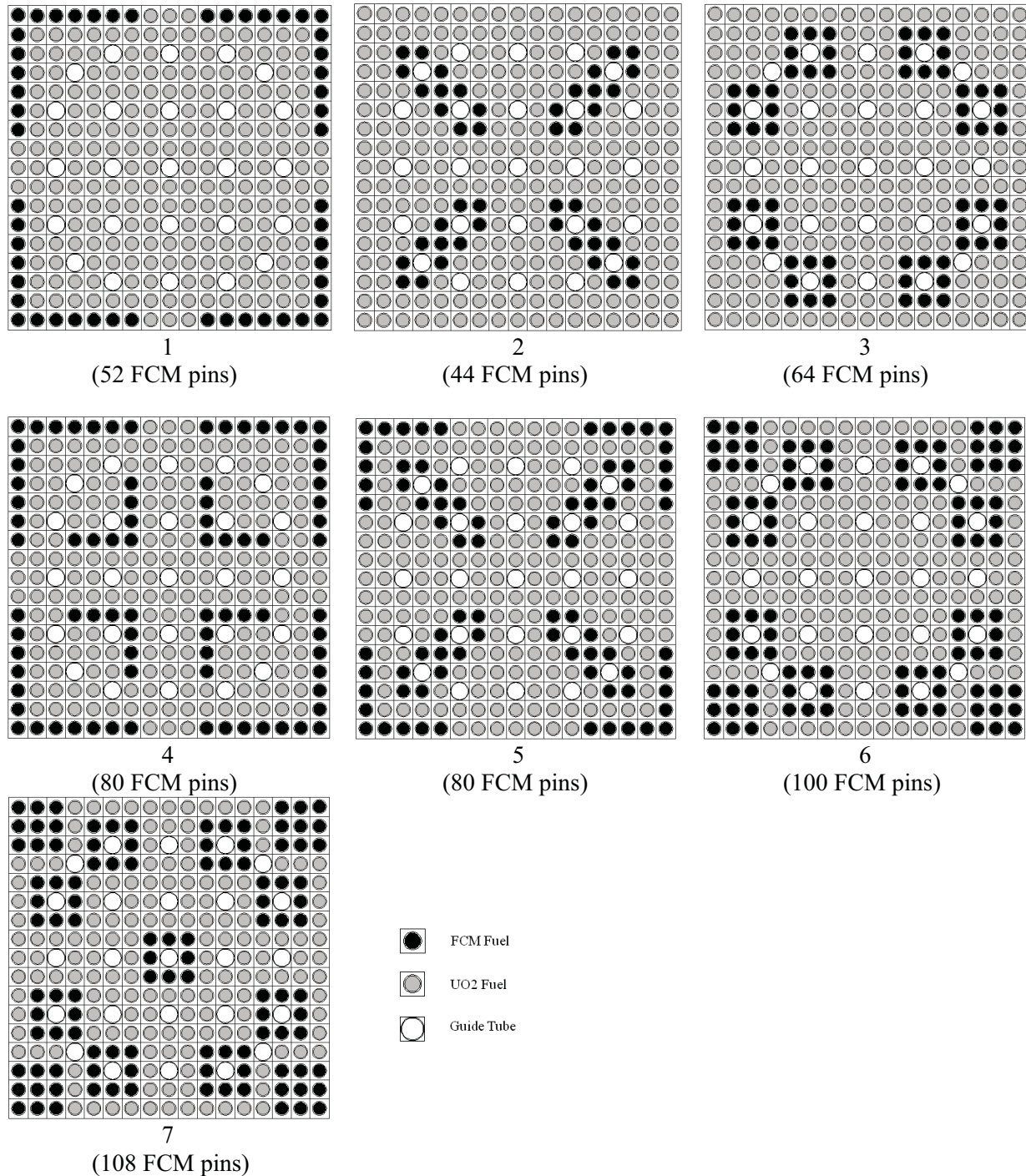


Figure 5-1. Arrangements of enriched UO<sub>2</sub> and TRU-only FCM pins in heterogeneous PWR assemblies.

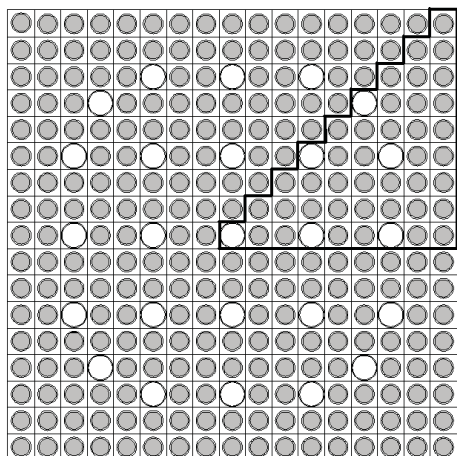


Figure 5-2. Diagram of fuel assembly showing the octant reported in subsequent pin power plots.

## 5.2 Results of Assembly Calculations

### 5.2.1 Pin Powers

The relative pin powers at four depletion points are given for the  $\text{UO}_2$  and MOX assemblies in Figure 5-3 and Figure 5-4, respectively.

In the  $\text{UO}_2$  case shown in Figure 5-3, one sees that the maximum power peak occurs at the beginning of irradiation and is located at a pin location adjacent to a control rod guide tube. This is due to the extra moderation provided by the additional water in the guide tube. As the assembly is burned, the power shape flattens as high-power pins burn out, shifting power to those originally at low relative power.

In the MOX case shown in Figure 5-4, results are similar to the  $\text{UO}_2$  case, only the peaking at beginning of irradiation is a bit more pronounced. This is a result of the large fission cross section of the plutonium exposed to the additional moderation of the water in the empty guide tubes. Again, the peaking is reduced with burnup as in the  $\text{UO}_2$  case.

Beginning with Figure 5-5 and continuing through Figure 5-11, pin power peaking values are again given for four points during irradiation for each of the heterogeneous  $\text{UO}_2$ /FCM assembly configurations 1 through 7. In Configuration 1 (shown in Figure 5-5), one sees that the power is low in the FCM pins at beginning of irradiation. This is due to the hard spectrum resulting from TRU-only FCM pins being located adjacent to each other. Late in the irradiation, the FCM pins have become depleted and their power fraction is low as peaking shifts even more to  $\text{UO}_2$  pins. In these figures, depletion points both early and late in the irradiation are shown in order to observe the burnup behavior and power sharing of pins. However, it is beginning of life peaking factor that is most important with regard to thermal hydraulic margins since the assembly will have the greatest power at this point.

Similar trends can be observed in the other heterogeneous  $\text{UO}_2$ /FCM assembly configurations, and detailed discussion will not be included for each. Note that in all cases, the beginning of irradiation peaking factors all fall below a value of 1.2, which is a typical limit for single-assembly scoping calculations of this kind. In the cases where larger numbers of FCM fuel are used, the peaking later in the irradiation becomes quite high. This is because the FCM pins are again quite depleted and the power burden is distributed among fewer  $\text{UO}_2$  pins. Configuration 7 is the most pronounced example of this effect.



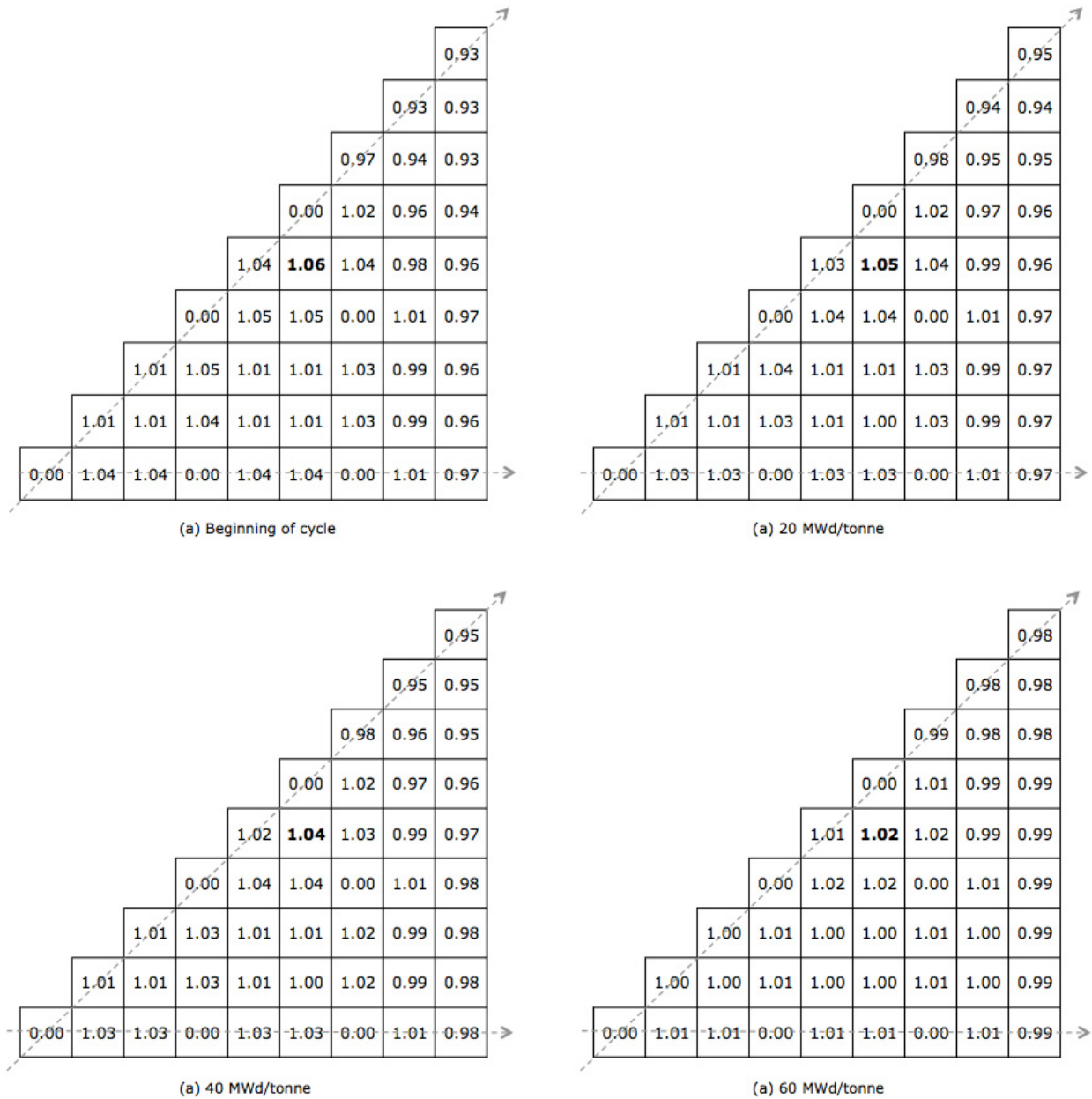


Figure 5-3. Relative pin powers at four points during irradiation for the UO<sub>2</sub>-only fuel assembly.

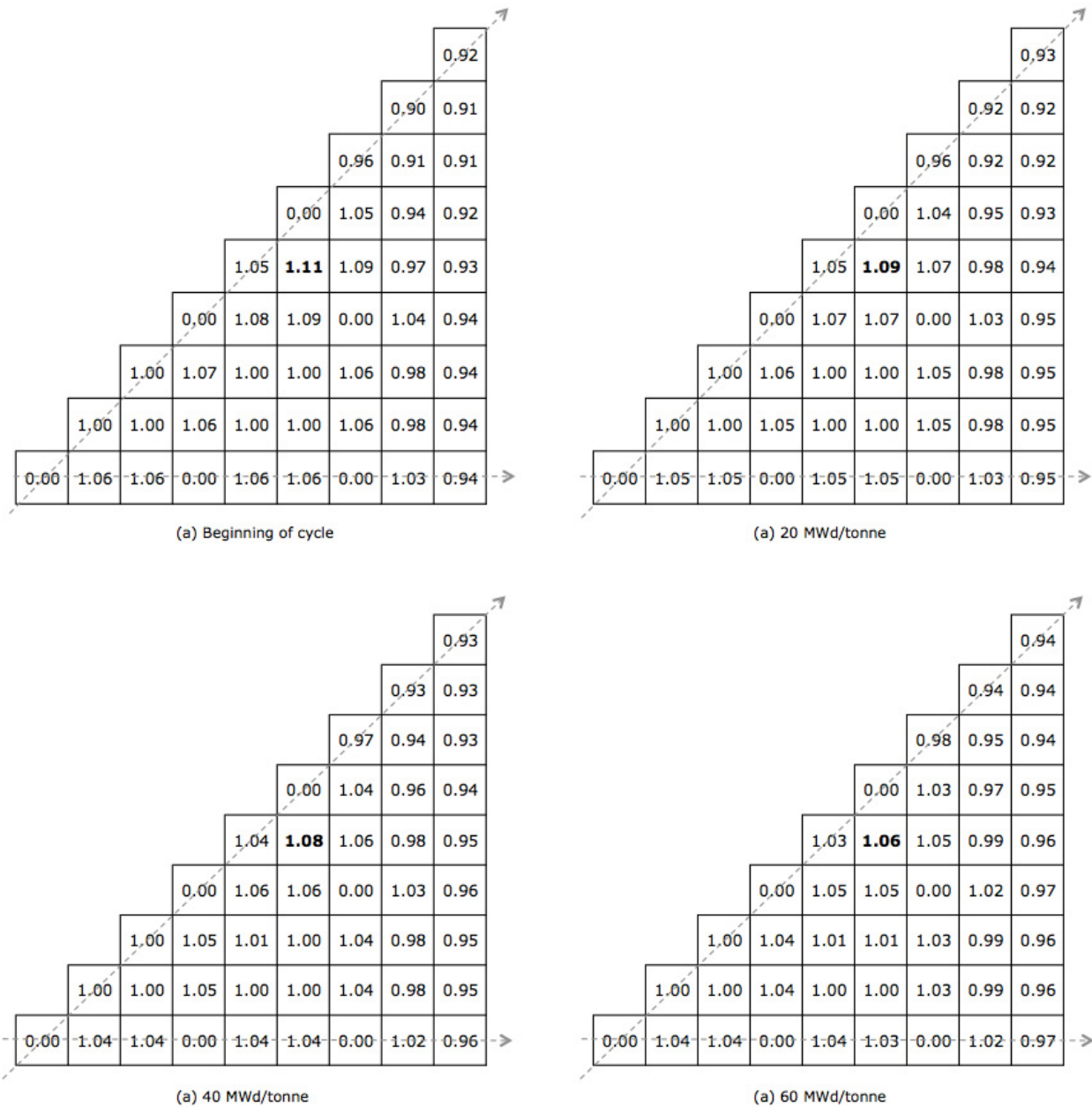


Figure 5-4. Relative pin powers at four points during irradiation for the MOX fuel assembly.

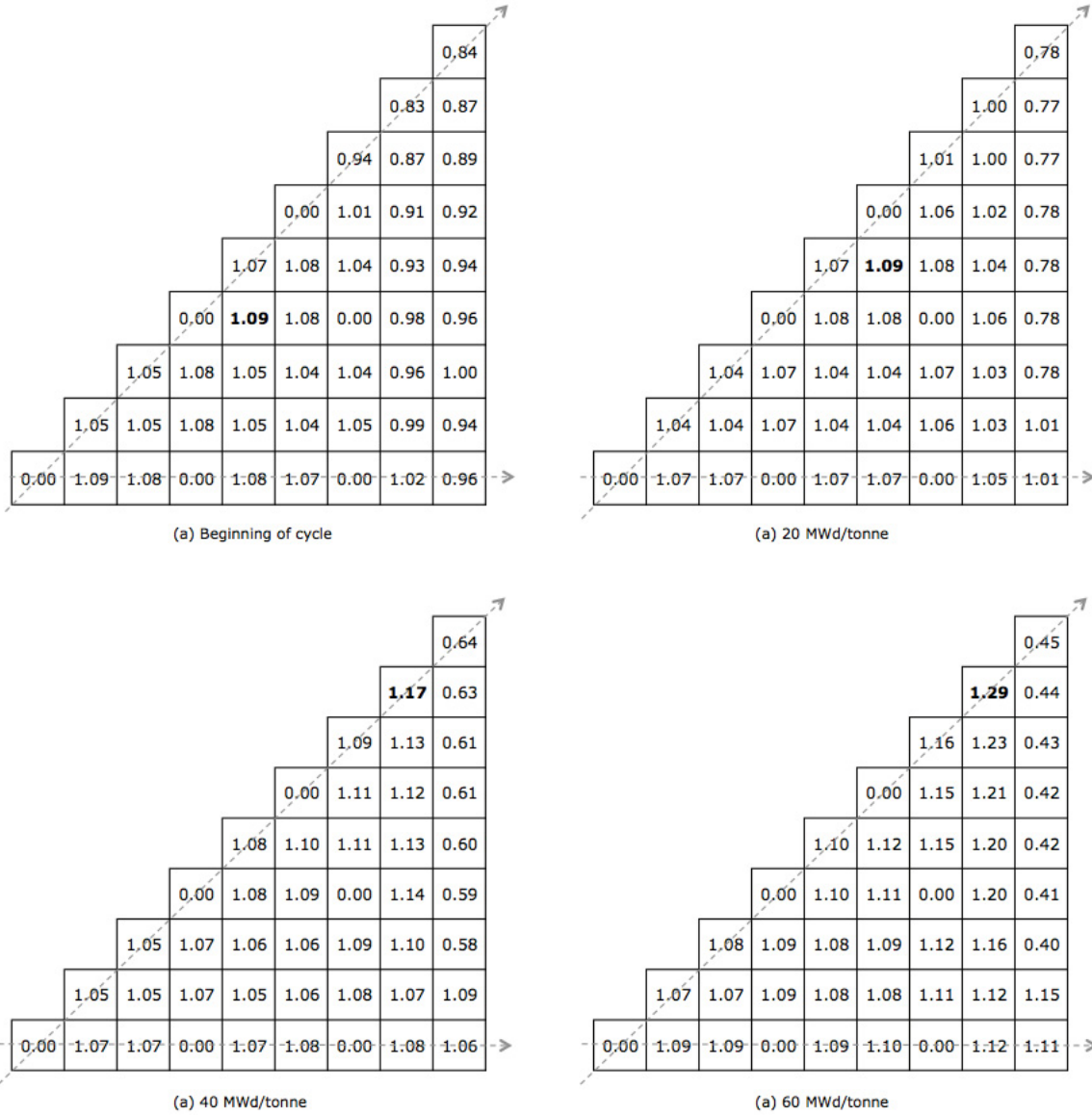


Figure 5-5. Relative pin powers at four points during irradiation for FCM configuration 1.

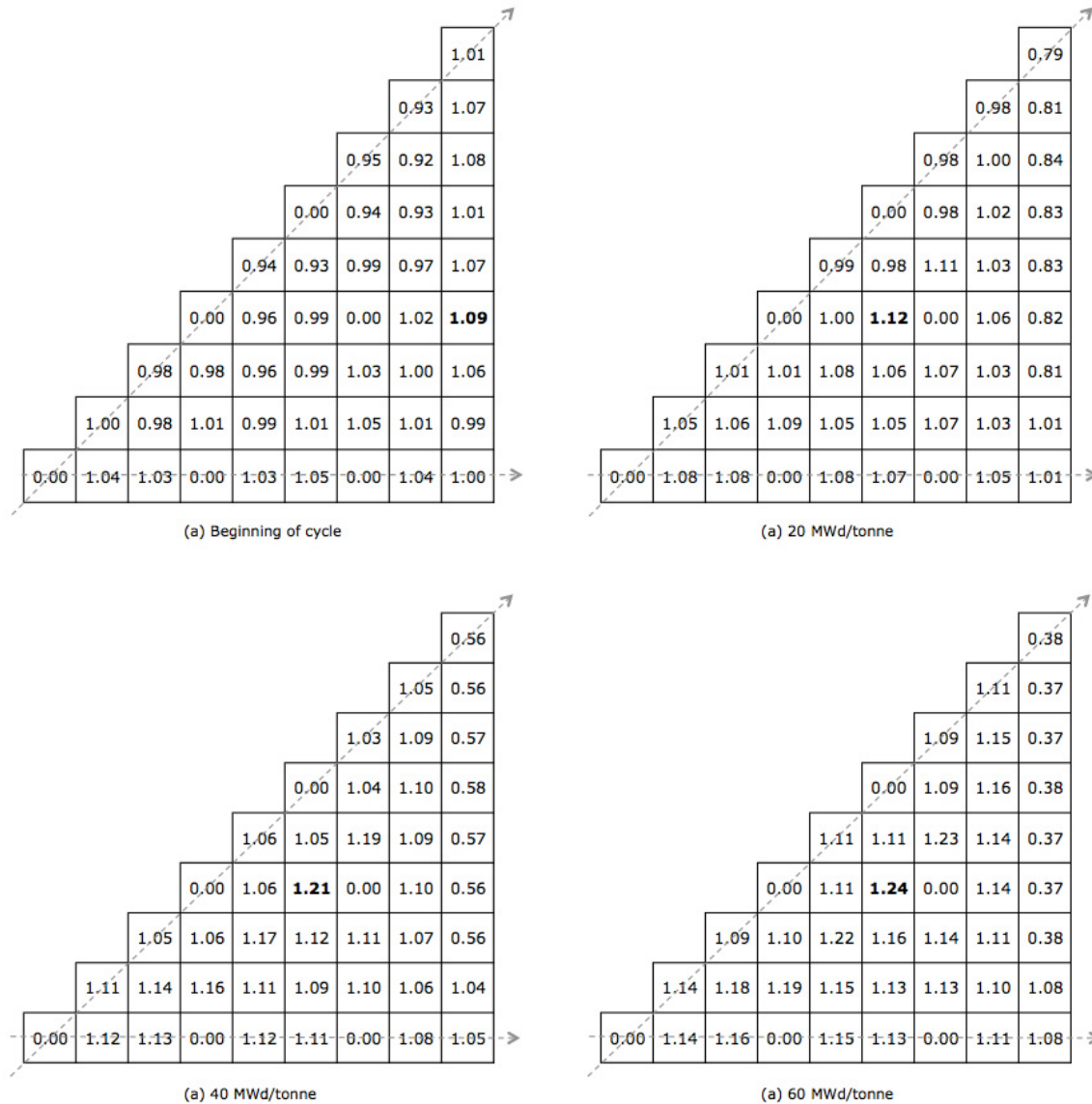


Figure 5-6. Relative pin powers at four points during irradiation for FCM configuration 2.

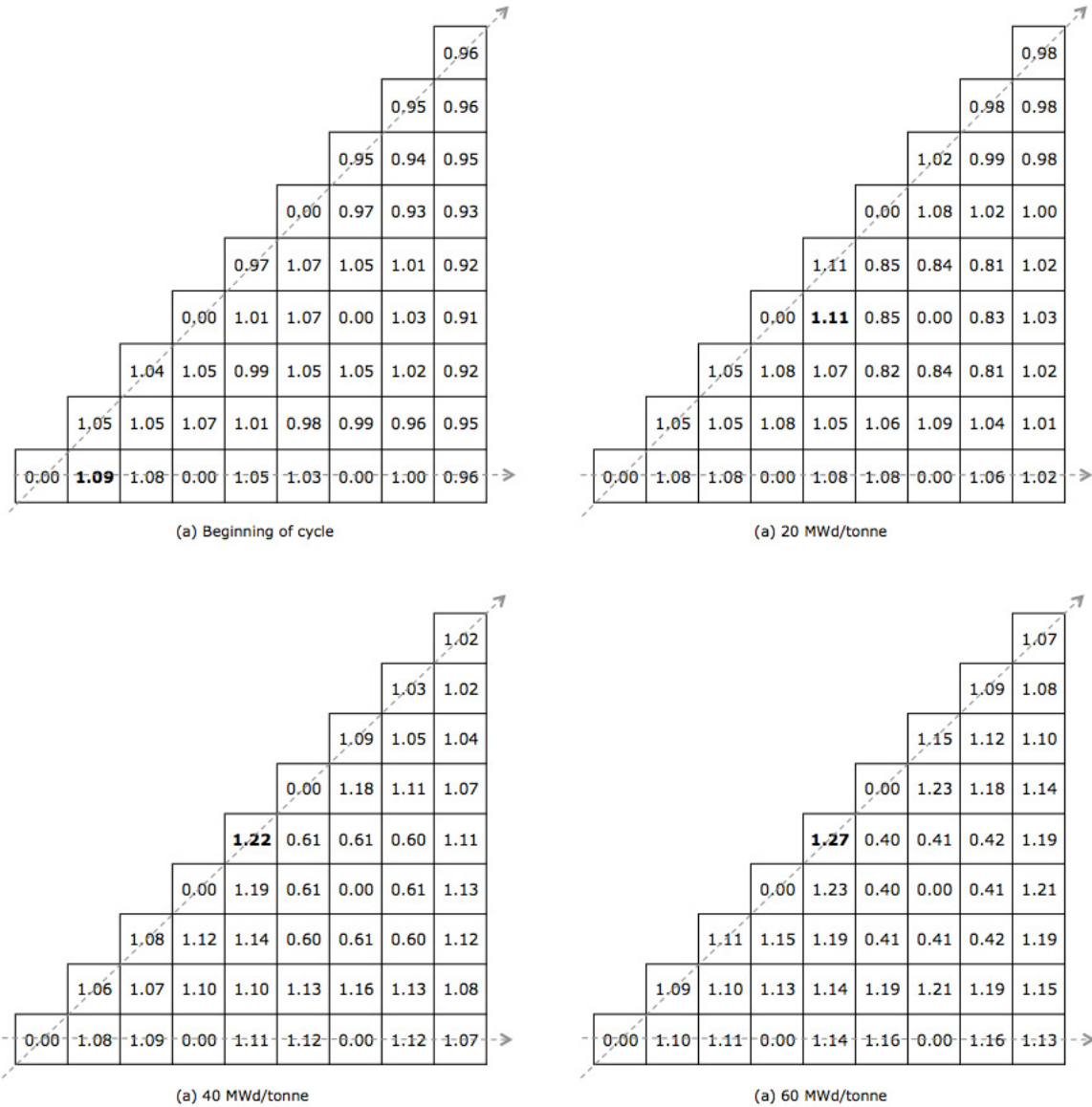


Figure 5-7. Relative pin powers at four points during irradiation for FCM configuration 3.

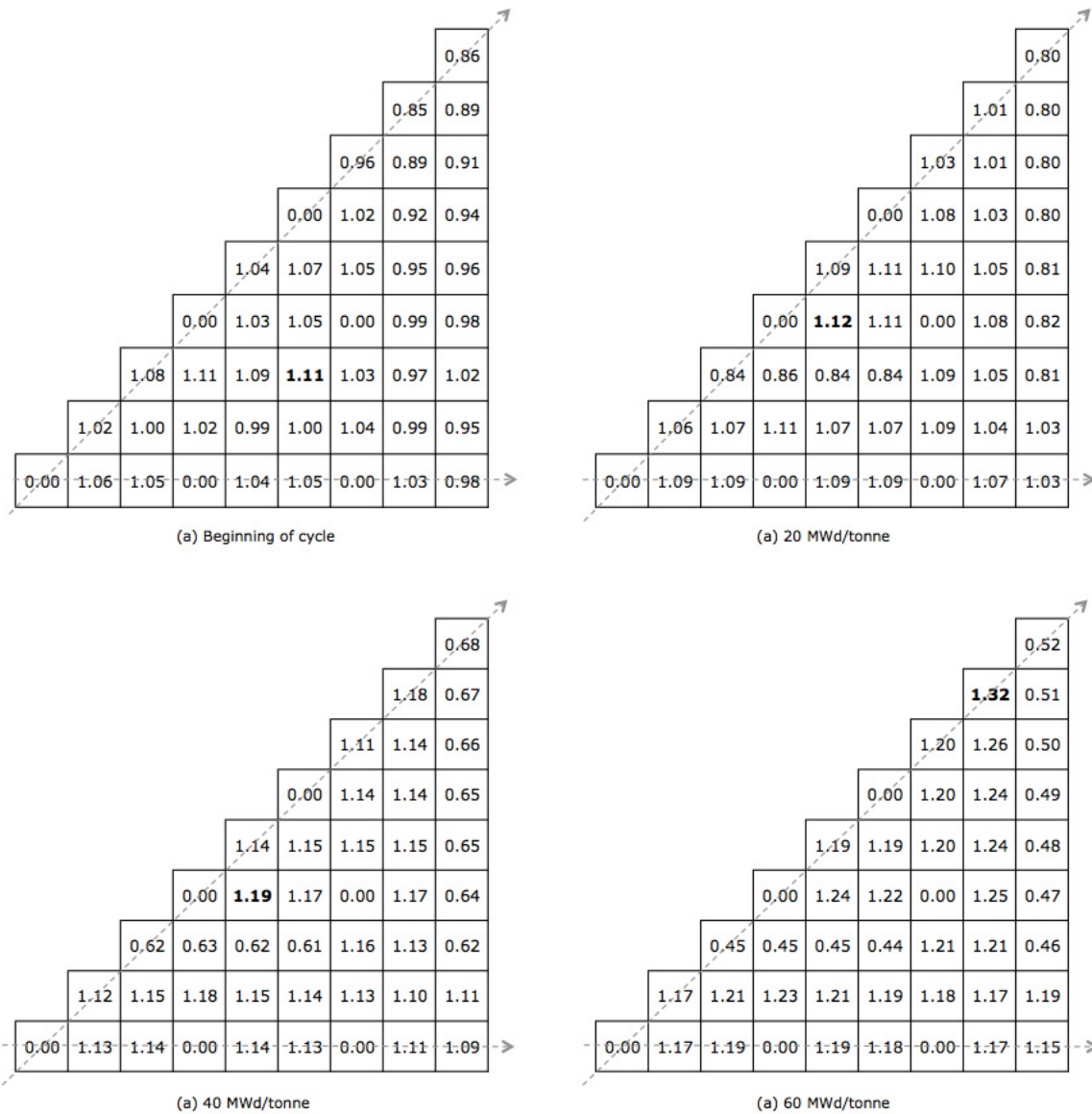


Figure 5-8. Relative pin powers at four points during irradiation for FCM configuration 4.



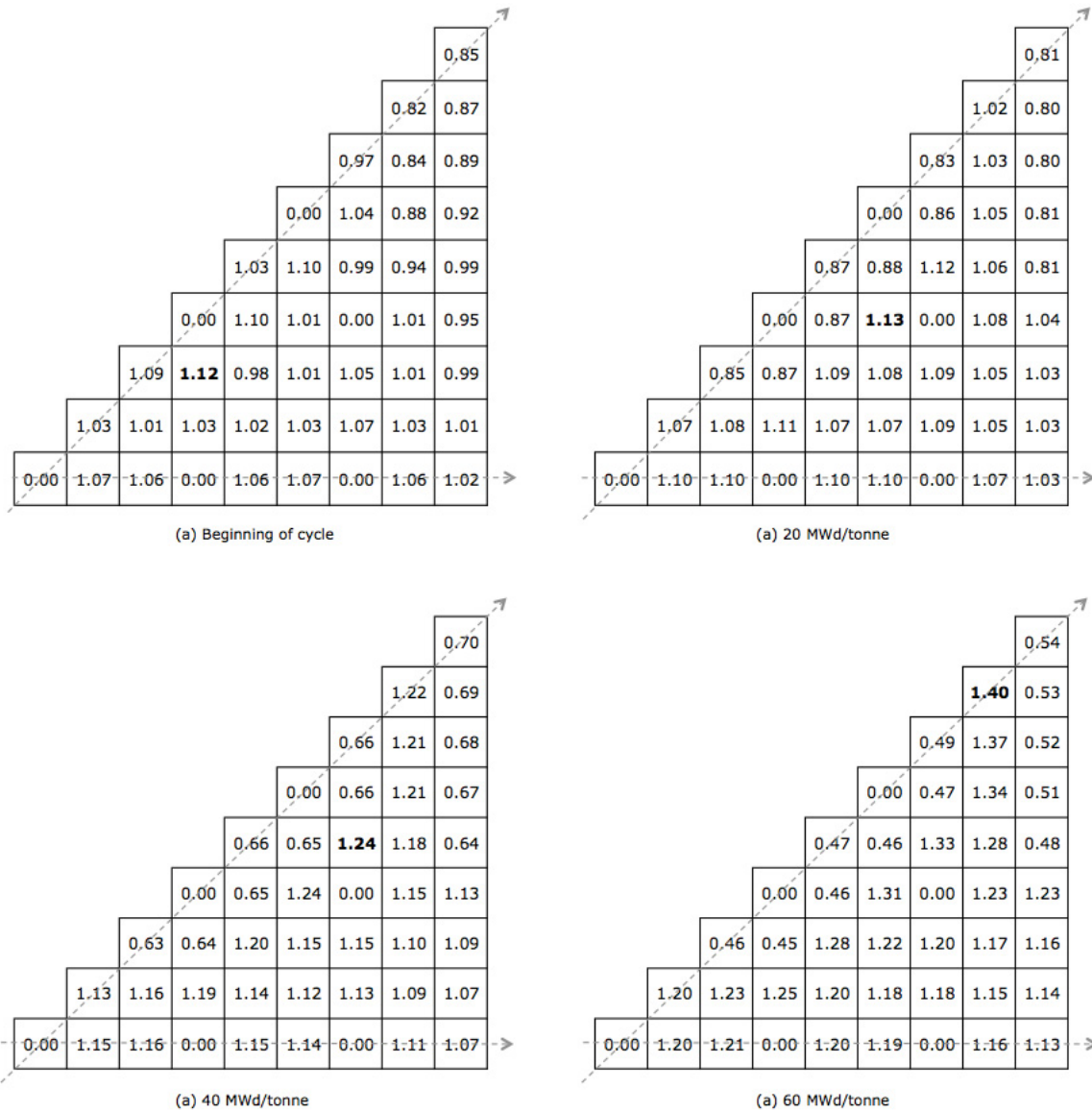


Figure 5-9. Relative pin powers at four points during irradiation for FCM configuration 5.

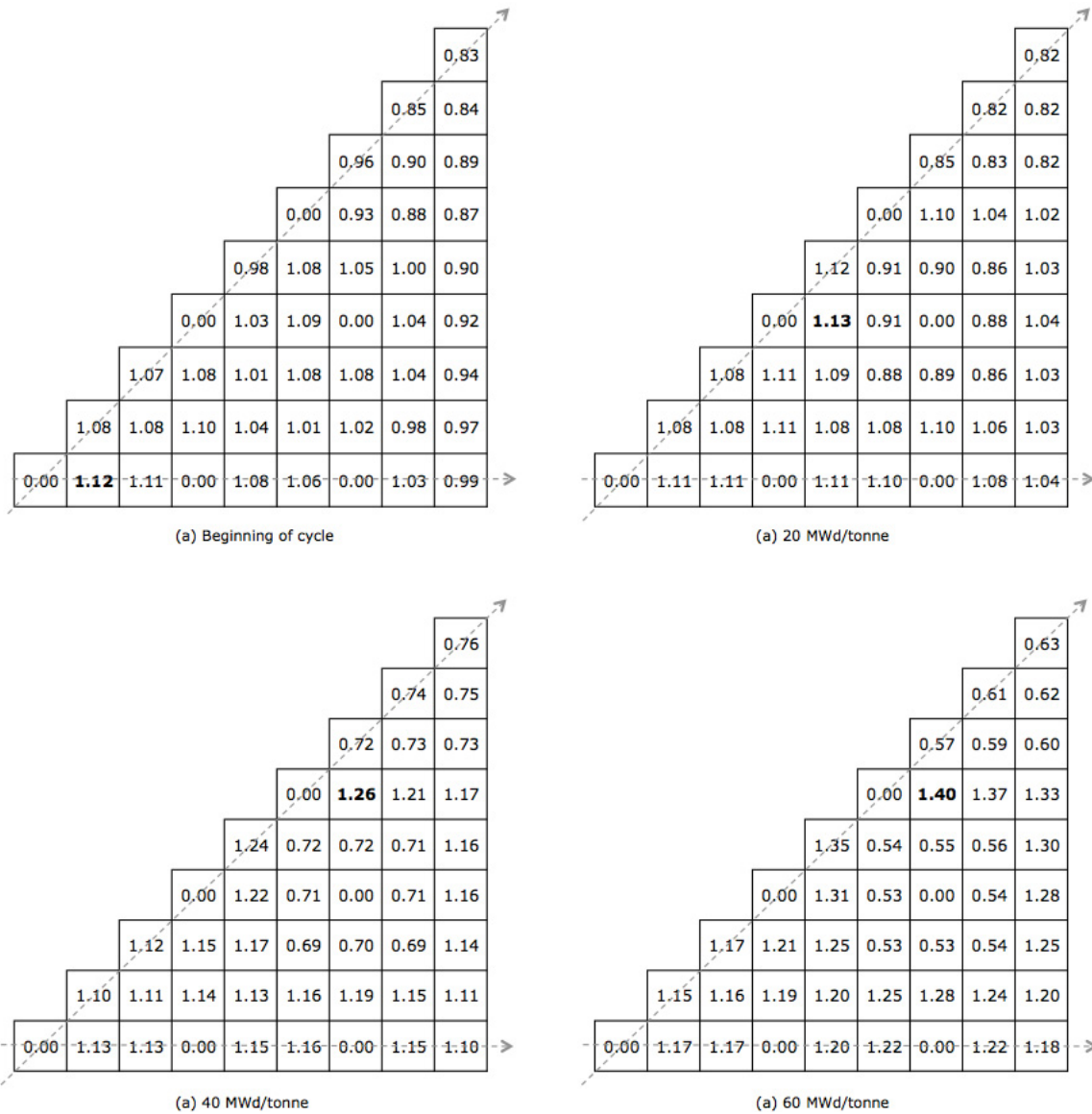


Figure 5-10. Relative pin powers at four points during irradiation for FCM configuration 6.



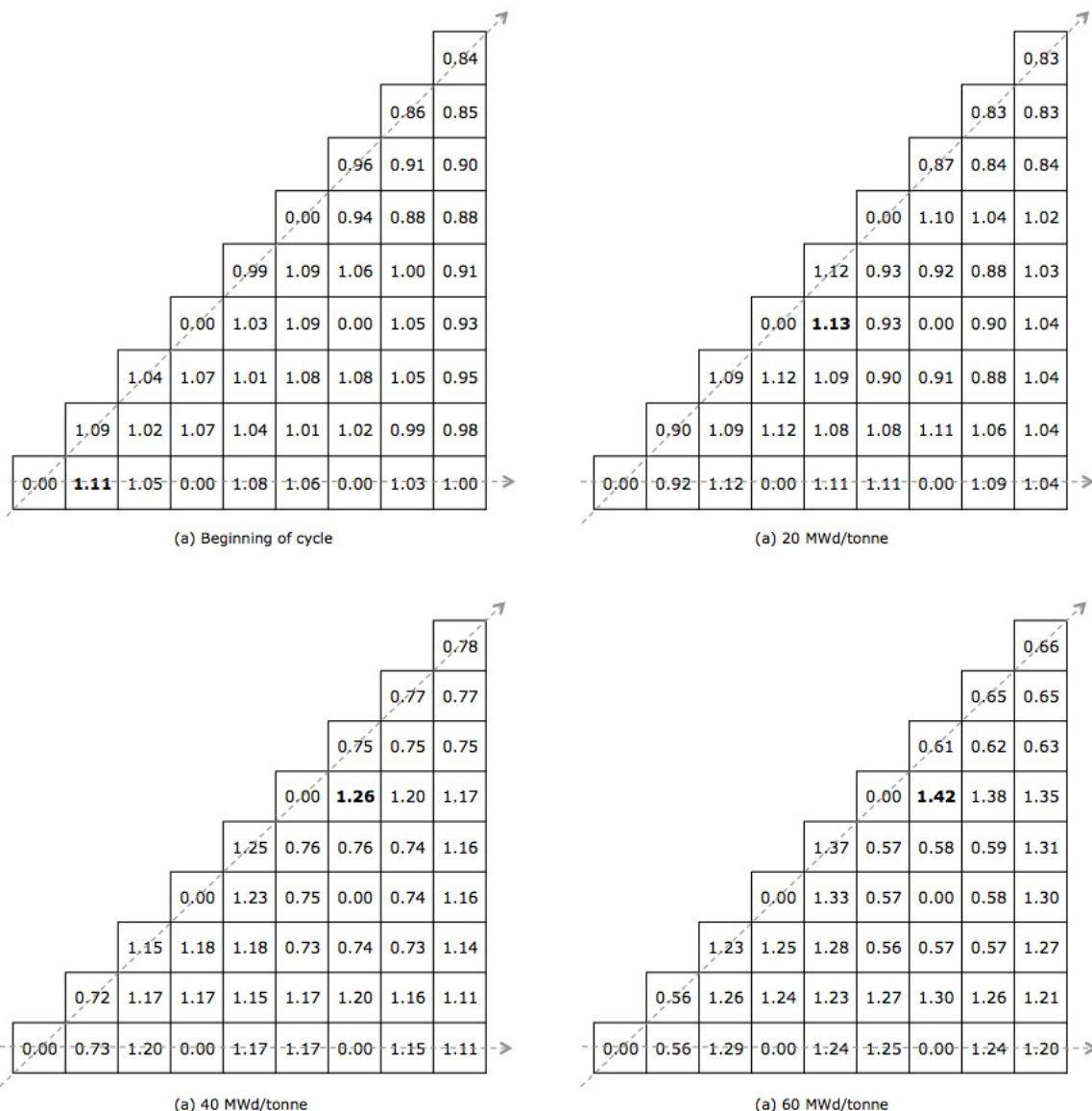


Figure 5-11. Relative pin powers at four points during irradiation for FCM configuration 7.

### 5.2.2 Reactivity-Limited Burnup and Coefficients

In this section, the reactivity-limited burnup and reactivity coefficients are examined for each of the heterogeneous  $\text{UO}_2/\text{FCM}$  configurations. Figure 5-12 shows  $k_\infty$  versus burnup in GWd/tonne for the  $\text{UO}_2$ -only assembly, the MOX-only assembly and the seven heterogeneous  $\text{UO}_2/\text{FCM}$  cases. The same data is plotted versus burnup in EFPD in Figure 5-13. These show that for all of the FCM cases, the burnup at which  $k_\infty$  crosses unity is slightly lower than the MOX and  $\text{UO}_2$  cases. However, the difference is not pronounced and the ability to reach acceptable cycle lengths in a 3-batch scenario should be preserved in any case.

Figure 5-14 and Figure 5-15 show MTC versus burnup for all the assembly cases analyzed. These show that while the MTC for the  $\text{UO}_2/\text{FCM}$  heterogeneous cases is less negative than the  $\text{UO}_2$ -only case, it is still negative to very high burnups and is, as expected, intermediate to the  $\text{UO}_2$ -only and the FCM unit cells in Section 4.2.

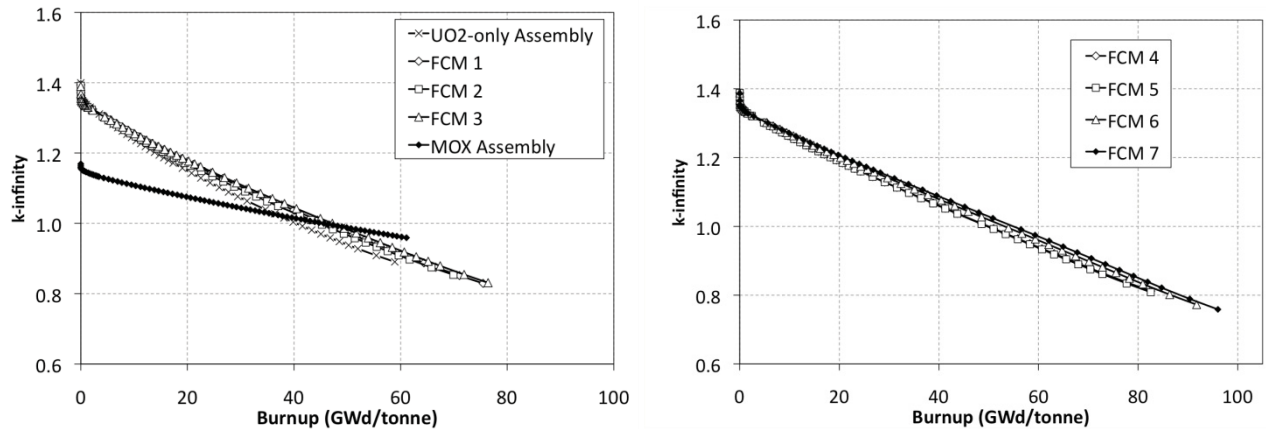


Figure 5-12.  $K_{\infty}$  versus burnup in GWd/tonne for UO<sub>2</sub>, MOX, and heterogeneous FCM/UO<sub>2</sub> assembly configurations.

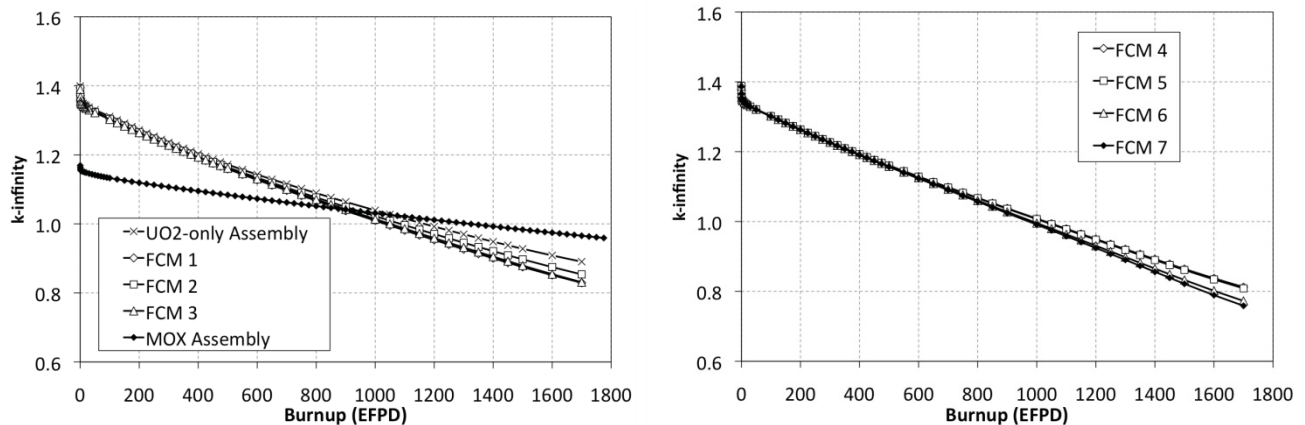


Figure 5-13.  $K_{\infty}$  versus burnup in EFPD for UO<sub>2</sub>, MOX, and heterogeneous FCM/UO<sub>2</sub> assembly configurations.

Figure 5-16 and Figure 5-17 show void coefficient (using 10% void case) versus burnup for all the assembly cases analyzed. These show that, like the MTC cases, the void coefficient for the UO<sub>2</sub>/FCM heterogeneous cases is less negative than the UO<sub>2</sub>-only case. However it is still clearly negative to very high burnups and is again intermediate to the UO<sub>2</sub>-only and the FCM unit cells in Section 4.2.

Figure 5-18 and Figure 5-19 show Doppler coefficient versus burnup for all the assembly cases analyzed. In these, the influence of the UO<sub>2</sub>-only cells on the Doppler coefficient of the overall assembly can be clearly seen as the values are much more negative than the unit cell TRU-only FCM cases of Section 4.

Finally, Figure 5-20 and Figure 5-21 give soluble boron worth versus burnup for all the assembly cases analyzed. The soluble boron worth for the UO<sub>2</sub>/FCM heterogeneous cases is quite similar to the UO<sub>2</sub>-only case.

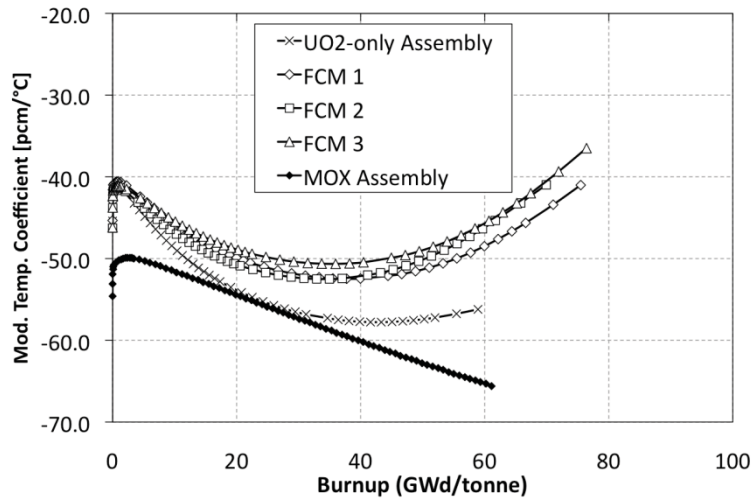


Figure 5-14. MTC versus burnup for UO<sub>2</sub>, MOX, and three heterogeneous FCM/UE assembly configurations.

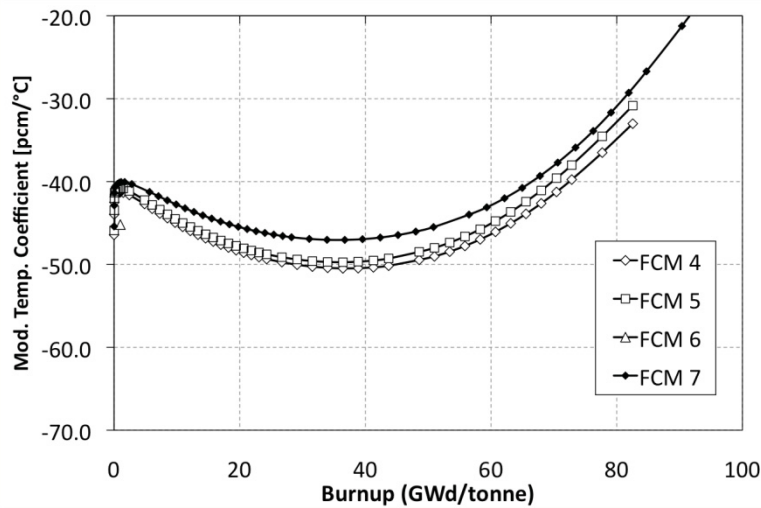


Figure 5-15. MTC versus burnup for four heterogeneous FCM/UE assembly configurations.

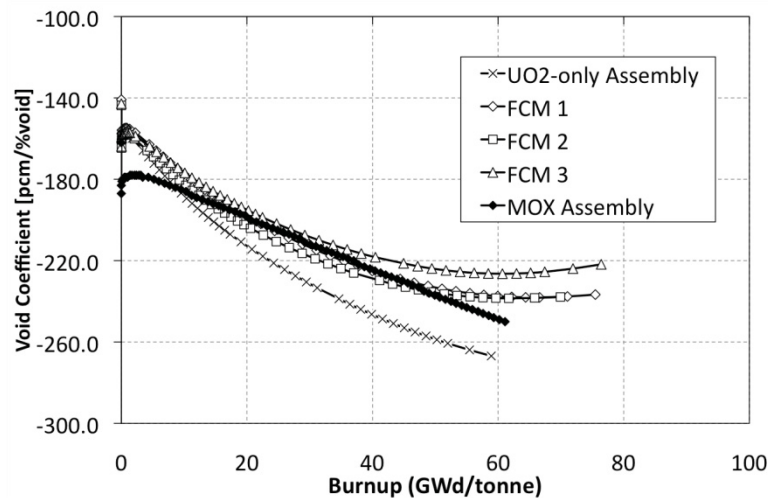


Figure 5-16. Void coefficient versus burnup for UO<sub>2</sub>, MOX, and three heterogeneous FCM/UE assembly configurations.

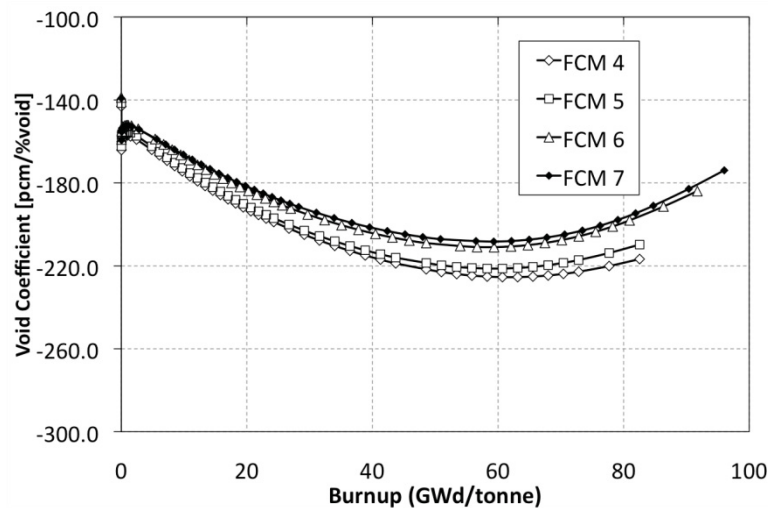


Figure 5-17. Void coefficient versus burnup for four heterogeneous FCM/UE assembly configurations.

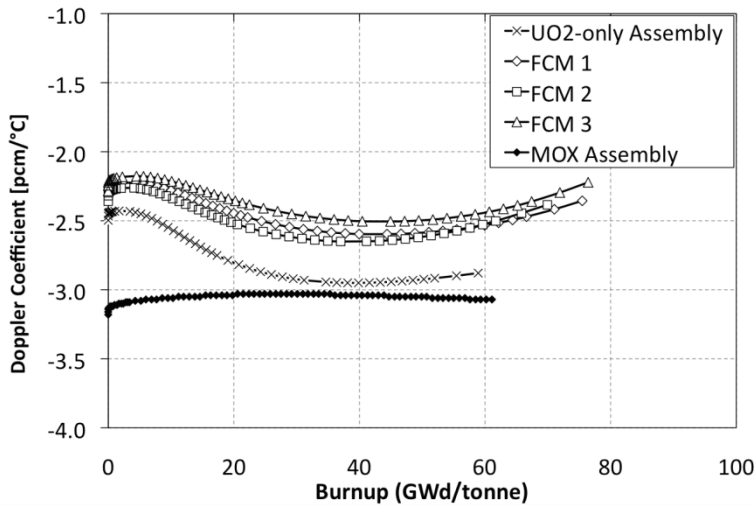


Figure 5-18. Doppler coefficient versus burnup for UO<sub>2</sub>, MOX, and three heterogeneous FCM/UO<sub>2</sub> assembly configurations.

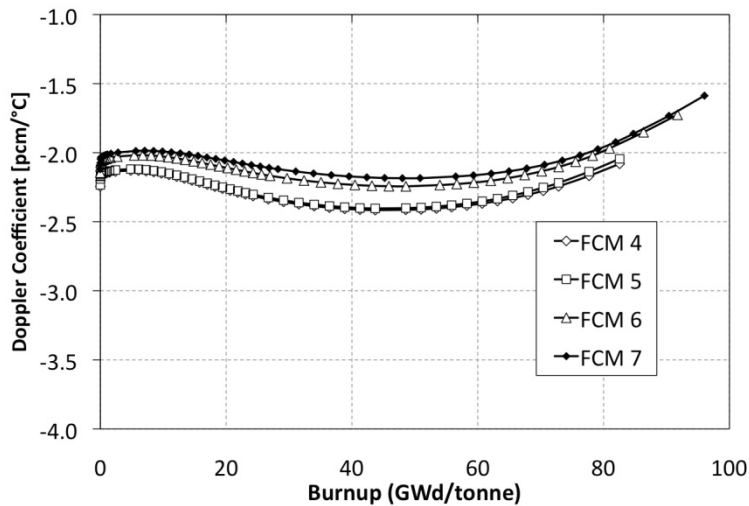


Figure 5-19. Doppler coefficient versus burnup for four heterogeneous FCM/UO<sub>2</sub> assembly configurations.

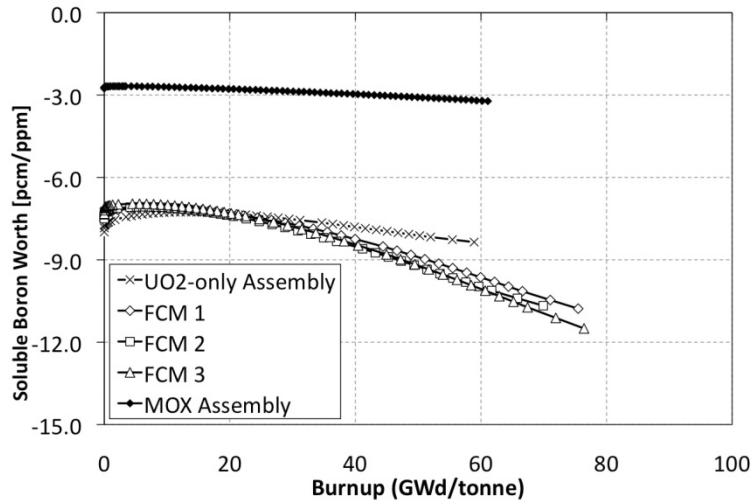


Figure 5-20. Soluble boron worth versus burnup for UO<sub>2</sub>, MOX, and three heterogeneous FCM/UE assembly configurations.

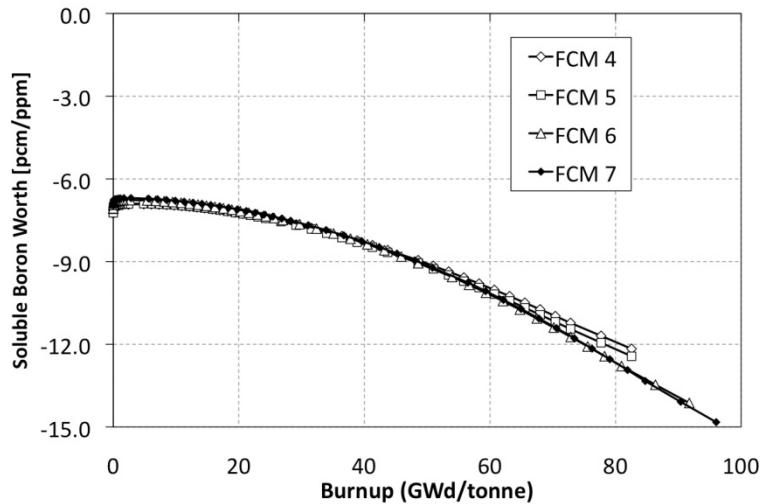


Figure 5-21. Soluble boron worth versus burnup for four heterogeneous FCM/UE assembly configurations.

While these neutronics calculations do not present any major issues that would disqualify any of the heterogeneous FCM/UE assembly configurations, other analyses must be performed in future work to ensure safety. One potential issue lies in the cases where TRU-only FCM fuel pins are placed near to or surrounding the empty guide tubes. If this is done in an assembly location where control rods will be inserted, the very low power in these pins toward the end of cycle may significantly degrade the control rod worth. More detailed assembly and whole-core calculations will have to be performed to ensure adequate rod worths.

In addition, some assumptions made in this work need to be replaced with detailed thermal analysis in order to provide a more reliable assessment of reactivity feedback. For example, the Doppler coefficient was calculated using the simplifying assumption that all fuel (TRISO particles, matrix, and UO<sub>2</sub> or MOX pellets) were operating at the same temperature and were perturbed to the same temperature. It is known

that the FCM fuel would have significantly different thermal conductivity than the  $\text{UO}_2$  or MOX pellets. Eventually, finite element models should be used to properly model the fuel temperatures in the FCM fuel.

### 5.3 Analysis of Complete Coolant Voiding

As was done in Section 4.4, analysis of complete coolant voiding was performed at the assembly level by plotting  $k^*$  versus fraction of nominal coolant density for each of the heterogeneous  $\text{UO}_2$ /FCM assemblies analyzed. These are all performed in an unirradiated condition. Figure 5-22 shows reactivity versus fraction of nominal coolant density for heterogeneous  $\text{UO}_2$ /FCM assembly configurations 1, 2 and 7. These represent the range of TRU-only FCM fuel pin numbers of all cases studied. This shows that, as predicted, the tendency for the  $\text{UO}_2$  pins to have large negative reactivity is carried to the heterogeneous assemblies. From these results, it appears that void reactivity is not a significant barrier to use of these heterogeneous assembly arrangements.

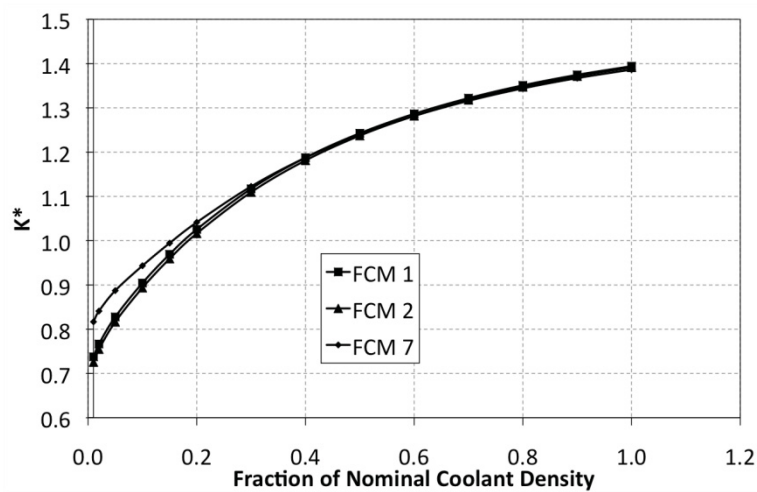


Figure 5-22. Reactivity versus fraction of nominal coolant density for four heterogeneous  $\text{UO}_2$ /FCM assembly configurations.

### 5.4 Fast Neutron Fluence

Like most nuclear fuels, performance of TRISO particle fuel is largely dictated by fast neutron fluence. This parameter was calculated for all FCM fuel pins in each of the heterogeneous FCM/ $\text{UO}_2$  assembly configurations analyzed above. Because the results of all of the cases are similar with respect to fast fluence, results for only one of the assemblies is shown in Figure 5-23. This plot gives fast fluence ( $>100$  keV) for the six FCM pins of heterogeneous assembly Configuration 2 versus burnup. Because fuel performance is not the main focus of this work, detailed discussion of the implications of the fast fluence on TRISO particle integrity are left to the companion report [B. Boer, et. al., FCR&D-2011-000338 or INL/EXT-11-23313]. However, it should be noted that these fluence values are quite high and exceed the region where data exists to supply the PASTA models. Further investigation should be devoted to more reliable modeling in this regime along with schemes for reduction of fast fluence.



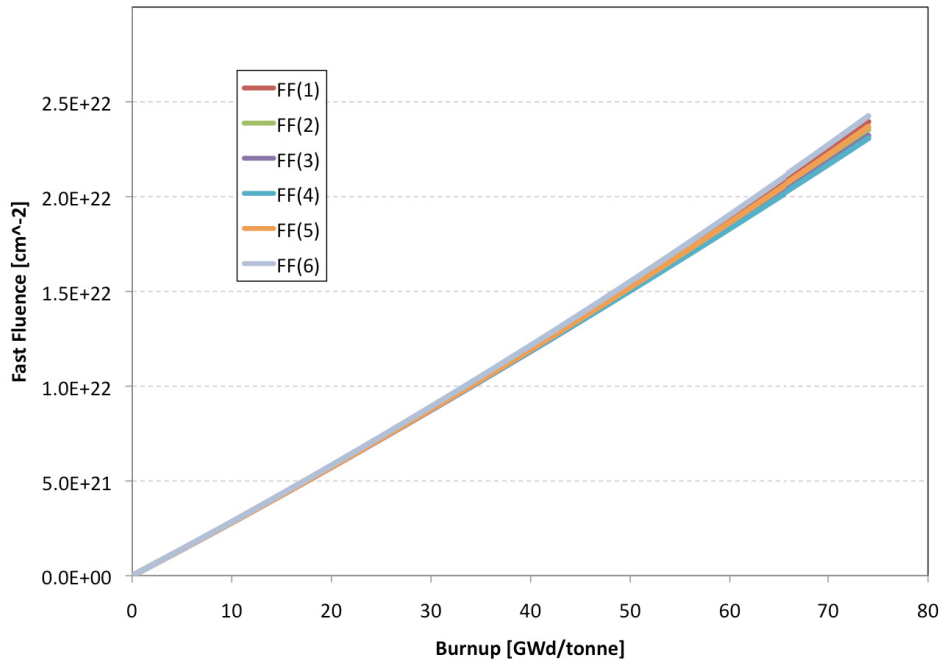


Figure 5-23. Fast fluence (>100 keV) versus burnup for the 6 FCM pin types in assembly configuration 2.

## 6. CONCLUSIONS AND FUTURE WORK

Unit cell and assembly calculations have been performed to assess the physics attributes of TRU-only FCM fuel in an LWR lattice. Various reactivity coefficients were calculated at each depletion step for comparison to reference unit cells containing typical  $\text{UO}_2$  and MOX.

It was shown that due to the limited space available for heavy metal loading in the FCM fuel, the reactivity-limited burnup (in days) at typical LWR power densities may be quite short if only FCM fuel is used. Thus, even before evaluating the reactivity feedback performance of the fuel, already the idea of heterogeneous assemblies containing pins of TRU-only FCM and LEU deserves consideration.

The reactivity parameters calculated at various levels of depletion are the MTC, the void coefficient (assuming 10% void), the Doppler coefficient, the soluble boron worth, and the reactivity effect of complete voiding of the coolant for both single unit cells of TRU-only FCM fuel and heterogeneous assemblies containing both  $\text{UO}_2$  and FCM pins.

### *Unit Cell Calculations*

Several different combinations of particle PF and kernel diameters were evaluated for the FCM fuel. It was found that the HM loading of the FCM fuel was the primary driver for reactivity-limited burnup and for reactivity coefficients, not how it is distributed in various kernel sizes and PF values. The MTC of the TRU-only FCM fuel was negative at beginning of life, but less so than the  $\text{UO}_2$  and MOX reference cases. As burnup increases, the MTC becomes less negative and in the cases with very small fuel loading eventually turns positive. The case with the smallest amount of fuel evaluated (500  $\mu\text{m}$  diameter kernel, PF = 20%, 0.21  $\text{g/cm}^3$  TRU) exhibits a positive MTC around a burnup of 200 GWd/tonne. This is because so little heavy metal remains that the system has become over-moderated. However, HM loadings this small are also undesirable from the standpoint of TRU destruction rates. In the higher loading cases, the MTC becomes positive at later, higher, burnup levels. Those levels are unlikely to be achieved.



The calculations of the void coefficient assuming 10% void showed similar results relative to the UO<sub>2</sub> and MOX reference cases. The value of this parameter for the TRU-only FCM fuel is negative at beginning of life, but less so than the UO<sub>2</sub> and MOX reference cases. With burnup, it becomes less negative, and in the cases with very small fuel loading, turns positive at higher burnup levels. The case with the smallest amount of fuel evaluated (500 µm diameter kernel, PF = 20%, 0.21 g/cm<sup>3</sup> TRU) gives a positive value around 400 GWd/tonne. Again, higher loadings than this are more desirable for TRU destruction reasons and a positive 10% void coefficient should be easily avoided.

The value of the Doppler coefficient for the fresh TRU-only FCM fuel is between -0.6 and -1.2 pcm/°C. With burnup, the magnitude of the Doppler coefficient of all FCM cases decreases until a value of 0 is reached at higher burnup levels. The burnup at which this occurs, as in the cases of MTC and 10% void, depends on the initial loading, and ranges from 350 to greater than 600 GWd/tonne. This is in contrast to the UO<sub>2</sub> and MOX cases, which remain at least as negative as -2.4 pcm/°C for the duration of their irradiation. Smaller, yet still negative, Doppler coefficients have advantages and disadvantages. The primary advantage is a lower reactivity swing from cold to hot full-power conditions, which translates into less reactivity demanding reactivity hold-down requirements. Disadvantages may include poorer (more severe) response to reactivity-initiated transients, such as a rod ejection or soluble boron dilution. Also, the uncertainty bands of very small negative Doppler coefficients can extend beyond zero into positive values.

Soluble boron worth calculations showed that the boron efficiency of the TRU-only FCM fuel was intermediate between the UO<sub>2</sub> and MOX cases. This is because although there is only TRU in the fuel, the spectrum is not as hard as in the case of the MOX fuel because of the very low HM loading. Consequently, the observed trend is that lower HM loading (through lower PF or kernel diameter) results in larger negative soluble boron worth. With burnup, the spectrum softens to a more thermal one than that of the UO<sub>2</sub> case, and so the soluble boron worth becomes quite large and negative. Therefore, soluble boron worth is not expected to be a significant design challenge for the TRU-only FCM fuel. Furthermore, control rod worth is not expected to be a significant issue with this fuel, though calculations at least at an assembly level should be used to verify this.

The analysis of the reactivity effects of 100% voiding suggests that the behavior of this fuel would be similar to MOX fuels of very high plutonium fraction, which are known to have positive void reactivity. In this preliminary assessment, no soluble or burnable poisons were used and no optimization of spectral effects has been attempted. The optimal balance of moderation, burnable poison loading and locations and soluble boron concentrations has yet to be explored. With the poisons in place in future lattice calculations at the assembly level, the void reactivity calculated will be more realistic. Further analysis will be performed at the assembly and whole core level in order to determine the void reactivity performance of the FCM fuel with such poisons in place.

The plutonium destruction performance of the TRU-only FCM fuel is attractive from the standpoint of the fraction of plutonium that is destroyed. This is a result of the absence of uranium and resulting inability to product more plutonium with irradiation. However, the amount of TRU that one may load in the FCM fuel is relatively small compared to ordinary MOX fuel.

#### *Heterogeneous Assembly Calculations*

If FCM fuel pins are included in a heterogeneous assembly alongside LEU fuel pins, the overall reactivity behavior is dominated by the uranium pins while attractive TRU destruction performance levels in the TRU-only FCM fuel pins may be preserved. Assembly calculations were performed on various heterogeneous FCM/UO<sub>2</sub> assembly configurations, specifically the effect of FCM pin locations on said worth. Overall, loadings of these types show promise from the standpoint of the reactivity-limited burnup and reactivity coefficients examined. However, some issues remain outstanding that should be examined in future work. These include control rod worth in heterogeneous FCM/UO<sub>2</sub> assembly configurations. Also, more detailed thermal analysis of the TRU-only FCM fuel pins should be conducted. Furthermore, it should be noted that the fast fluence values calculated in this work are quite high and exceed the region

where data exists to supply the PASTA models. Further investigation should be devoted to more reliable modeling in this regime along with schemes for reduction of fast fluence.

## 7. REFERENCES

1. R.M. Versluis, F. Venneri, D. Petti, L. Snead, D. McEachern, "Project Deep-Burn: Development of Transuranic Fuel for High-Temperature Helium-Cooled Reactors," *Proc. HTR 2008*, Washington D.C., USA, 28 Sept. – 1. Oct. (2008).
2. B. Boer, A. Ougouag, "Core Analysis, Design and Optimization of a Deep-Burn Pebble Bed Reactor," *Proc. PHYSOR-2010*, Pittsburgh, Pennsylvania, USA, 9 May – 14 May 2010.
3. Y. Kim, F. Venneri, "Optimization of One-Pass Transuranic Deep Burn in Modular Helium Reactor," *Nuclear Science and Engineering* 160, No. 1, p. 59, 2008.
4. D.A. Petti, D.A., J. Buongiorno, J.T. Maki, R.R. Hobbins and G.K. Miller, "Key Differences in the Fabrication, Irradiation and High Temperature Accident Testing of US and German TRISO-Coated Particle Fuel, and their Implications on Performance," *Nuclear Engineering and Design*, **222**, Issues 2-3, pp. 281-297, December (2002).
5. W.J. Carmack, M. Todosow, M.K. Meyer, and K.O. Pasamehmetoglu, "Inert Matrix Fuel Neutronic, Thermal-Hydraulic, and Transient Behavior in a Light Water Reactor," *Journal of Nuclear Materials*, **352**, pp. 276-284 (2006).
6. E. Shwageraus, P. Hejzlar, and M.S. Kazimi, "Optimization of the LWR Nuclear Fuel Cycle for Minimum Waste Production," MIT Report MIT-NFC-TR-60, October (2003).
7. M. Visosky, Y. Shatilla, P. Hejzlar, and M.S. Kazimi, "Actinide Transmutation in PWRs Using CONFU Assemblies," *Nuclear Science and Engineering*, **163**, pp. 215-242 (2009).
8. Boer, B., A.M. Ougouag, J.L. Kloosterman and G.K. Miller, "Stress Analysis of Coated Particle Fuel in Graphite of High-Temperature Reactors," *Nuclear Technology*, **162**, June (2008).
9. Venneri, F., et al., "High Temperature Reactor (HTR) Deep Burn Core and Fuel Analysis: Design Selection for the Prismatic Block Reactor," Idaho National Laboratory, INL/EXT-10-19973, September 29, 2010.
10. G.F. Sengler, F. Foret, G. Schlosser, R. Lisdat, and S. Stelletta, "EPR Core Design," *Nuclear Engineering and Design*, **187**, pp. 79-119 (1999).
11. R.N. Morris and P.J. Pappano, "Estimation of Maximum Coated Particle Fuel Compact Packing Fraction," *Journal of Nuclear Materials*, **361**, pp. 18-29 (2007).
12. G. Youinou, G. Puill, A. Guigon, and B. Giriend, "Plutonium Management and Multirecycling in PWRs using the Enriched Uranium Support," *Proceedings of GLOBAL '99*, Jackson Hole, Wyoming (1999).
13. G. Marleau, A. Hébert, R. Roy, "A User Guide for DRAGON Version 4," IGE-294, École Polytechnique de Montréal, October, 2008.
14. A. Hébert, "A Collision Probability Analysis of the Double-Heterogeneity Problem," *Nuclear Science and Engineering*, **115**, No. 2, p. 177, 1993.

15. N. Hfaiedh, A. Santamarina, "Determination of the Optimized SHEM Mesh for Neutron Transport Calculations," Proc. Mathematics and Computation, Supercomputing, Reactor Physics and Nuclear and Biological Applications, Avignon, France, 12 Sept. – 15 Sept. (2005).
16. L.L. Snead, et. al., "Handbook of SiC Properties for Fuel Performance Modeling," *Journal of Nuclear Materials*, **371**, pp. 329-377 (2007).
17. J.C. Maxwell, -Garnett. Phil. Trans. Roy. Soc. Lond., A 203, p. 385, 1904.
18. J.J. Duderstadt, and L.J. Hamilton, Nuclear Reactor Analysis, pp. 475-482.
19. D. Olander, Fundamental Aspects of Nuclear Reactor Fuel Elements, 1976.
20. D.G. Martin, "Considerations Pertaining to the Achievement of High-Burnups in HTR Fuel," *Nuclear Engineering and Design*, **213**, pp. 241-258 (2001).
21. Barbrault, P., "A Plutonium-Fueled High-Moderated Pressurized Water Reactor for the Next Century," *Nuclear Science and Engineering*, Vol. 122, pp. 240–246, 1996.
22. Kloosterman, J. L. and E. E. Bende, "Plutonium Recycling in Pressurized Water Reactors: Influence of the Moderator-to-fuel Ratio," *Nuclear Technology*, 130, 227, 2000.
23. Puill, A. and J. Bergeron, "Advanced Plutonium Fuel Assembly: An Advanced Concept for Using Plutonium in Pressurized Water Reactors", *Nuclear Technology*, 119, 119, 1997.
24. Sakurada, K., Motoo, A., Takashi, K., et al., "Studies on Advanced PWR Cores for Effective Use of Plutonium and Analysis of MOX Physics Experiments," *Proceedings of GLOBAL '99*, Jackson Hole, Wyoming. American Nuclear Society, LaGrange Park, Illinois, 1999.
25. Girieud, R., B. Guigon, R. Lenain, N. Barbet, and E. Royer, "A 100% MOX Core Design Using a Highly Moderated Concept," *Proceedings of GLOBAL '97*, Yokohama, Japan, 1997.
26. Ledergerber, G., C. Degueudre, U. Kasemeyer, A. Stanculescu, J. M. Paratte, and R. Chawla, "Using Civilian Plutonium in LWRs with an Inert Matrix Fuel (IMF)," Proc. Int. Conf. Future Nuclear Systems (GLOBAL'97), Yokohama, Japan, October 5–10, 1997, p. 1068, 1997.
27. Paratte, J. M. and R. Chawla, "On the Physics Feasibility of LWR Plutonium Fuels without Uranium," *Annals of Nuclear Energy*, Vol. 22, No. 7, pp. 471–481, 1995.
28. Kasemeyer, U., J. M. Paratte, P. Grimm, and R. Chawla, "Comparison of Pressurized Water Reactor Core Characteristics for 100% Plutonium-Containing Loadings," *Nuclear Technology*, Vol. 122, 52, 1998.
29. Youinou, G., "Advanced Pu Management Strategies in PWRs," Presentation at the 2003 Frédéric Joliot/Otto Hahn Summer School, Forschungszentrum Karlsruhe, Germany, August 20–29, 2003.
30. Aniel, S., J. Bergeron, and A. Puill, "Evaluation of the Maximum Plutonium Content of a MOX-Fuelled Pressurized Water Reactor Versus Isotopic Composition with Respect to the Void Coefficient," IAEA-TECDOC-941, International Atomic Energy Agency, 1997.